6. Nuclear Magnetic Resonance (NMR) Spectroscopy.

In this chapter we will discuss some basic principles of NMR spectroscopy and some very basic applications. A comprehensive treatment of NMR spectroscopy would require a separate series of lectures in 1 or even 2 semesters. This introduction will make beginners familiar with the ideas behind the NMR technique and the application of the method to smaller molecules.

6.1. The Magnetic Resonance Experiment.

6.1.1 Spin and magnetic moment of nuclei in an applied magnetic field.

As we have already pointed out for previously discussed techniques, the interaction of electromagnetic radiation with matter requires a change in the dipole moment of the molecule that interacts with the radiation. In optical and infrared spectroscopy, a change of the electrical dipole moment in the molecule was caused by the electrical field vector of the radiation. Magnetic resonance phenomena are interactions between the magnetic field vector of the electromagnetic radiation and the magnetic dipole of the molecule. Since the magnetic and the electric field vector are in phase, the frequency of the change in the magnetic field vector is the same as the frequency of the electrical field vector (just the frequency of the electromagnetic radiation). Absorption occurs if the energy difference between the magnetic dipole moment of the molecule in the ground state and the magnetic dipole moment in the excited state is equal to hν.

The magnetic resonance phenomenon is based on the fact that elementary particles have a property called “spin”, which is often seen as a rotation of the particle around its axis. It was shown by quantum theory that for example electrons have two spin states. This was experimentally first observed in absorption spectra of sodium, where the so called sodium D absorption line has a doublet fine structure (the line is split because of the angular momentum of the electron in the excited state (3p), that induces a magnetic field towards which the magnetic field induced by the spin can be parallel or antiparallel. Thus absorption takes place to different energy levels, depending on the spin of the electron in the excited state (in the electronic ground state 3s, the electron does not have an angular momentum).

In nuclear magnetic resonance the spin of the nucleus of an atom induces a magnetic dipole moment. Spin and magnetic dipole moment are proportional

$$\vec{\mu}_I = g_N \gamma_N \vec{I} \qquad \text{Eq. 6.1}$$

The constant

$$\gamma_N = \frac{q}{2m} \qquad \text{Eq. 6.2}$$

is termed the magnetogyric ratio of the particle.

The constant g_N is specific for a nucleus. For example, a free proton has the value g_N=5.585. In the presence of an external magnetic field, the nucleus of interest can be in to different energetic states that are given by *the dipole moment of the nucleus and by the magnitude of the external magnetic field.* The energy of the nucleus is then

$$E = \vec{\mu} \cdot \vec{B}_0 = g_N \gamma_N \vec{I} \cdot \vec{B}_0 \qquad \text{Eq. 6.3}$$

Quantum theory shows that the spin can be conveniently expressed by a spin quantum number I, that gives rise to an angular momentum. This angular momentum is of the magnitude:

$$\vec{I} = \sqrt{I(I+1)}\hbar \qquad \text{Eq. 6.4}$$

Nucleus	Mass	Charge	Spin	Natural abundance (%)	Relative sensitivity
^{1}H	1	1	1/2	99.98	1.000
^{2}H	2	1	1	0.016	0.0096
^{12}C	12	6	0	98.96	-
^{13}C	13	6	1/2	1.11	0.016
^{14}N	14	7	1	99.64	0.001
^{15}N	15	7	1/2		
^{16}O	16	8	0		-
^{17}O	17	8	5/2		
^{19}F	19	9	1/2	100	0.834
^{31}P	31	15	1/2	100	0.066
^{32}S	32	16	0	95.06	-

Table 1 The nuclear spin originates from the protons and the neutrons. Nuclei with odd mass and even charge number often have no spin, while nuclei with even mass and odd charge number often have a spin of 1/2 or an odd multiple of 1/2.

The spin of a charge particle gives rise to a magnetic dipole moment:

$$\vec{\mu}_I = g_N \gamma_N \vec{I} = g_N \gamma_N \sqrt{I(I+1)}\hbar = g_N \beta_N \sqrt{I(I+1)} \qquad \text{Eq. 6.5}$$

The constant $\beta_N = \gamma\hbar$ is the so called Bohr Magneton of the nucleus.

The spin quantum number I is specific for the particle of interest. It can be only *one* value (depending on the particle) out of the set 0, 1/2, 1, 3/2, 2, 5/2, ... (Table 1).

In a magnetic field, the spins of the charged particles precess around the z-axis that is defined by the direction of the magnetic field (Figure 6.1). The frequency by which the spins precess

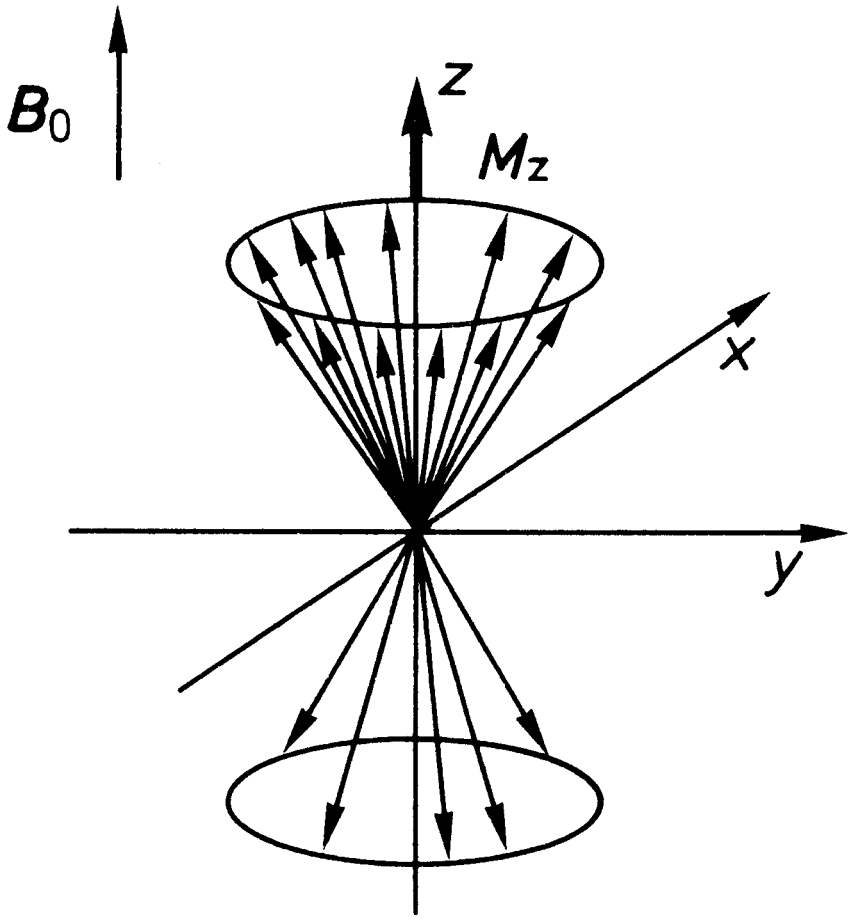

Precession of a group of identical nuclei in a magnetic field. The field causes a macroscopic magnetization in the direction of the applied magentic field, which defines the z-direction. In x and y direction, there is a statistical ditribution of the nuclei and thus no macroscopic magnetization.

Figure 6.1 Precession of spinning nuclei around the direction of a magnetic field B_0.

around the magnetic field vector is called Larmor frequency and given by

$$\omega = \frac{\text{magnetic moment}}{\text{angular momentum}} B_0 = \frac{\mu B_0}{2\pi I} = \frac{g\beta_N}{h} B_0, \text{ (expressed in Hz)}$$

Eq. 6.6

The directions that the spin can take in a magnetic field depend on the spin quantum number of the nucleus (Figure 6.2).

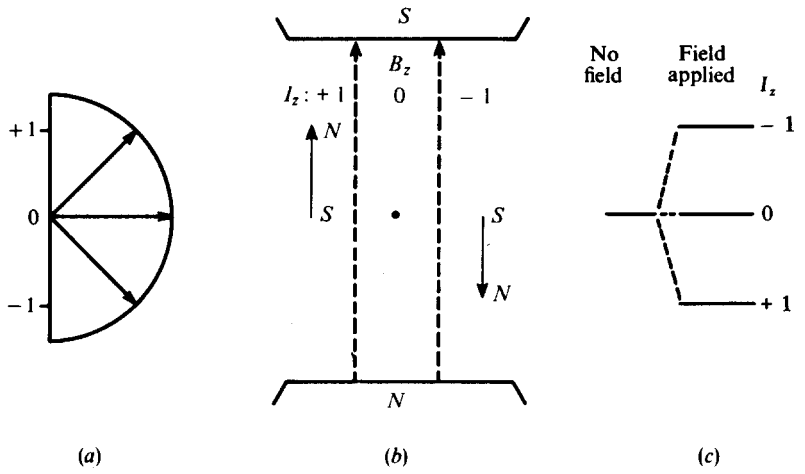

A nucleus with spin quantum number I=1 can have three orientations (a). In a magnetic field the magnetic dipole of the spinning nucleus will orient itself in three possible directions (b) that correspond to three energetic states of the nucleus (c).

Figure 6.2 Possible orientations of the magnetic dipole moments of precessing nuclei with spin quantum number I=1 with respect to a magnetic field.

Nuclei with a quantum number of I=1 can have components in the direction of the magnetic field that are m_I=–1, m_I=0, and m_I=+1. In general, nuclei with an integral spin quantum number I can have the z-components

$$m_I = I, I-1,..., 0, ...–(I-1), –I \text{ ; for I integral}$$

while nuclei with a spin quantum number that is a half-integral number can have the z-components

$$m_I = I, I-1, ..., 1/2, –1/2, ..., –I \text{ ; for I as an odd multiple of 1/2.}$$

which gives 2I+1 components in each case. These components are degenerate in absence of a magnetic field, but split into different energy levels if a magnetic field is present. The component of the magnetic dipole moment of the precessing spins that is parallel to the

magnetic field B_0
is then given by:

$$\mu_z = g_N \beta_N m_I \qquad \text{Eq. 6.7}$$

For a nucleus with a spin quantum number I=1, the angular momentum is given by

$$|I| = \sqrt{I(I+1)}\hbar = \sqrt{2}\hbar \qquad \text{Eq. 6.8}$$

with a corresponding magnetic moment of

$$\mu_I = g_N \beta_N |I| = g_N \beta_N \sqrt{I(I+1)} = g_N \beta_N \sqrt{2}. \qquad \text{Eq. 6.9}$$

The vector component in z-direction of such a spin will take the values of m_I = –1, 0, or +1 (from quantum mechanics). The orientation of the spin that corresponds to m_I=–1 has a magnetic dipole that is opposed to the applied external magnetic field B_0. Thus, this state corresponds to a higher energy level than the magnetic dipole of the I=+1 resonance line.

For a nucleus with I=1/2 we obtain in analogy m_I = –1/2, +1/2 and an angular momentum of the spinning nucleus is given by

$$|I| = \sqrt{I(I+1)} = \sqrt{\frac{1}{2}\left(1+\frac{1}{2}\right)} = \frac{1}{2}\sqrt{3}, \qquad \text{Eq. 6.10}$$

which corresponds to a magnetic momentum of

$$\mu_I = g_N \beta_N |I| = g_N \beta_N \sqrt{I(I+1)} = g_N \beta_N \sqrt{3}/2 \qquad \text{Eq. 6.11}$$

with a z-component in an external magnetic field of

$$\mu_z = +\frac{1}{2} g \beta_N \text{ or } \mu_z = -\frac{1}{2} g \beta_N. \qquad \text{Eq. 6.12}$$

In an external magnetic field, these two orientations of the magnetic dipole moment correspond to two energy levels that are

$$E = -\vec{\mu} \cdot \vec{B} = -\frac{1}{2} g_N \beta_N B_0 \text{ and } E = -\vec{\mu} \cdot \vec{B} = +\frac{1}{2} g_N \beta_N B_0 \qquad \text{Eq. 6.13}$$

For a transition from the energetically preferred state to the higher energy level, the sample has to be irradiated by radiation of such energy. The resonance condition is then:

$$\Delta E = g_N \beta_N B_0 = h\nu \qquad \text{Eq. 6.14}$$

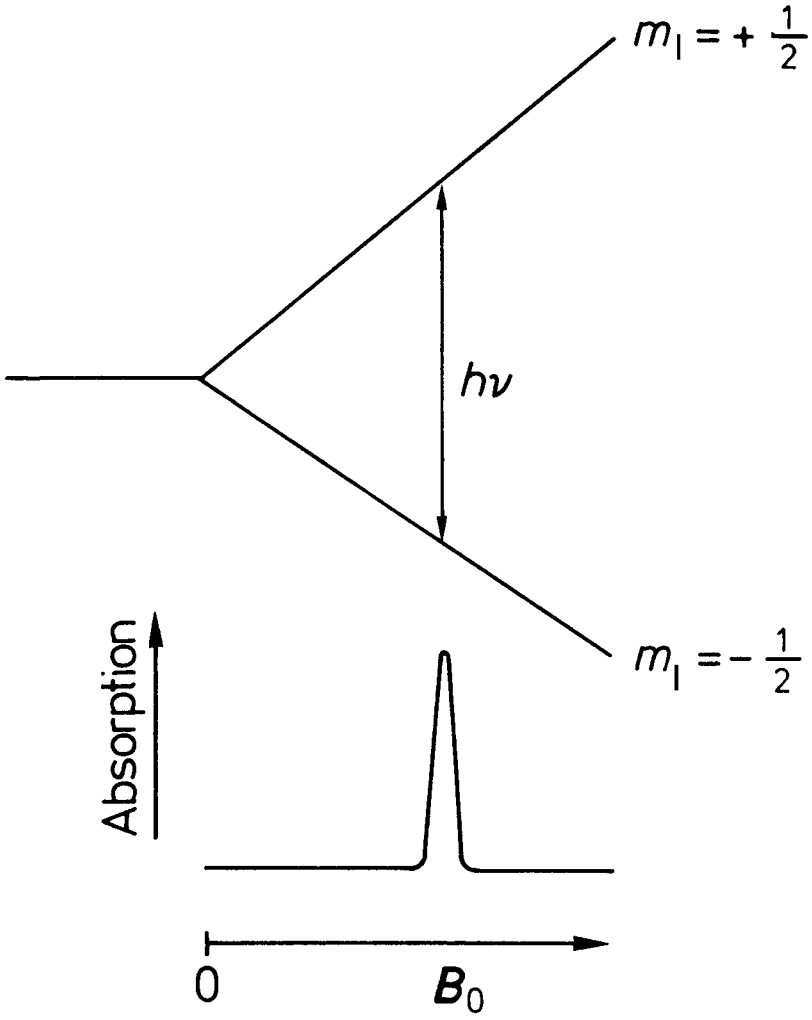

The resonance frequency in a magnetic resonance experiment depends on the strength of the magnetic field B_0 .

Figure 6.3 The resonance frequency depends on the strength of the magnetic field B0.

6.1.2 The resonance experiment

The interaction between the spinning nucleus and the incident radiation therefore strictly requires an external magnetic field and the absorption frequency of magnetic resonance is dependent on the strength of the applied magnetic field (illustrated in Figure 6.3). How does resonance take place ?

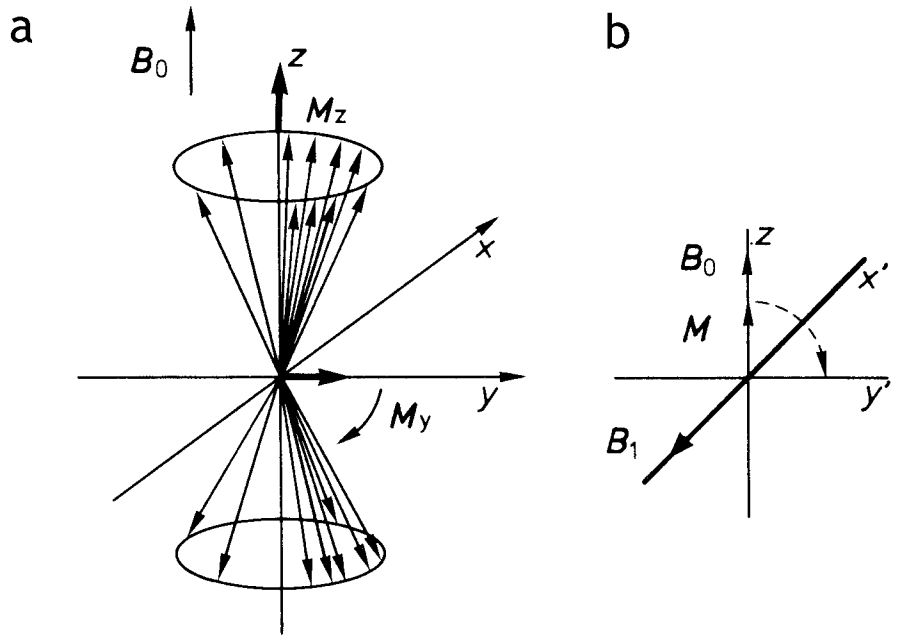

a Effect of a B_1-field that is oriented in x-direction. The forced phase coherency of the spins induces a transverse magnetization M_y in y-direction.

b Precession of the magnetization along the direction of the B_1-field (that defines the x' direction of the rotated coordinate system.)

Figure 6.4 Effect of the radio wave B_1 field on the nuclei precessing around the direction of the external B_0 field.

When the external field B_0 is applied, the nuclear spins orient themselves such that they are precessing around an axis that is defined by the magnetic field vector $\vec{B}_0$ with the Larmor frequency. Most nuclei will orient themselves such that their magnetic moment is directed parallel to the $\vec{B}_0$ field vector. Some of them will orient themselves antiparallel to the $\vec{B}_0$ field. The orientation of the nuclear spin in the $\vec{B}_0$ field also defines the direction of the precession of the spin. There is now a macroscopic magnetization M_z in z-direction that is caused by the nuclei of the substance in the field. While the spins are all precessing with the Larmor frequency, there is no phase coherence between them, i.e. their position on the precession cone is random (Figure 6.4). This also means, that there is no magnetization in x or in y direction. In an NMR experiment a linearly polarized radio wave radiation (typically of a frequency between 60 MHz and 1 GHz) is now directed towards the sample. The

magnetic field vector $\vec{B}_1$ of this radiation oscillates in x-direction. In our discussion of CD-spectroscopy, we have seen that a linearly polarized changing magnetic field can be decomposed into two circularly polarized components. These are characterized by two rotating magnetic field vectors in the x-y plane, which rotate in opposite directions. If the resonance condition is met the circularly polarized component that rotates in the direction of the precessing spins will force some of the spins to be phase coherent. The field $\vec{B}_1$ rotates with the Larmor frequency

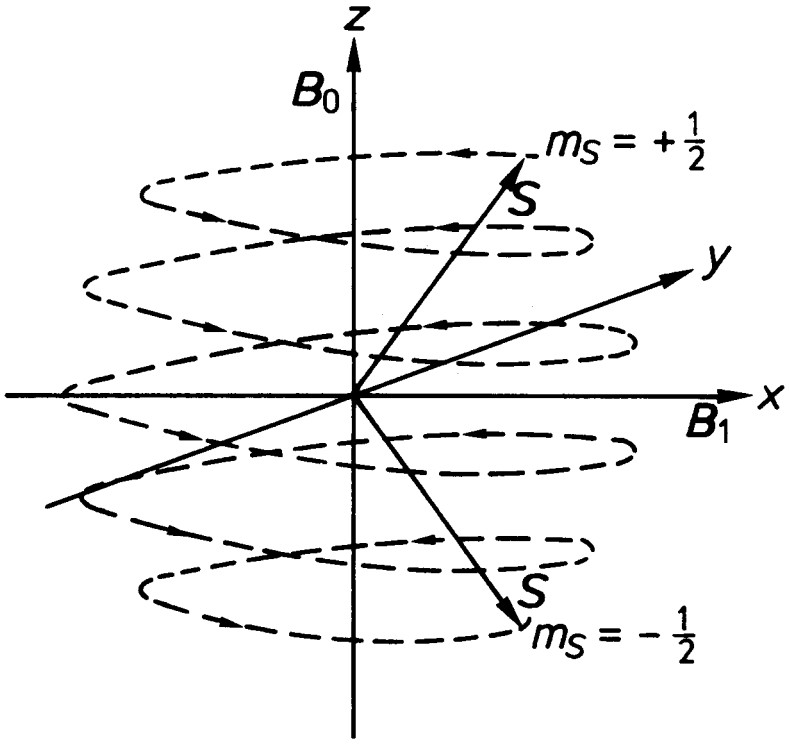

Superposition of the precessions around the direction of B_0-field (z-axis) and the B_1 -field. The B_1-field rotates with the Lamor frequency around the z-axis. Precession around the axis of the B_1 -field is slower because of B_1 is smaller than B_0.

Figure 6.5 Superposition of the spin precession around the z- and around the x-axes. induced by the magnetic field vecors B_0 and B_1.

and induces such partial phase coherence and thus a magnetization M_y perpendicular to $\vec{B}_0$ which oscillates in the x, y plane with the Larmor frequency (Figure 6.4). A receiver coil that is positioned along the y-direction detects the voltage that is induced by the rotating magnetization vector (M_y) and detects when absorption of the radiation occurs. To imagine the absorption process we view the coordinate system as rotating with the Larmor frequency around the z-axis. The rotating axes are know designated x' and y'. The advantage of a rotating coordinate system is that now the magnetic field vector $\vec{B}_1$ is stationary in the

direction of x'. The magnetization in z-direction is affected by the $\vec{B}_1$ field and a torque

$$T = \vec{M}_z \times \vec{B}_1 \qquad \text{Eq. 6.15}$$

is exercised, which is perpendicular to the directions of both $\vec{B}_0$ and $\vec{B}_1$ and therefore in y-direction, giving rise to a magnetization in y'-direction (Figure 6.4). As a consequence, more spins are driven to an antiparallel orientation with respect to $\vec{B}_0$. If a resonant $\vec{B}_1$ field is irradiating the sample, a precession of a magnetization vector around the direction of the $\vec{B}_1$-field axis is induced (Figure 6.5).

6.1.3 The NMR spectrometer.

In practice, the NMR-spectrometer operates at a fixed frequency of the radio wave radiation (i.e. a fixed frequency of the $\vec{B}_1$ field, for instance 500 MHz) and the strength of the B_0 field is altered (field sweep). A scheme of the NMR spectrometer is depicted in Figure 6.6.

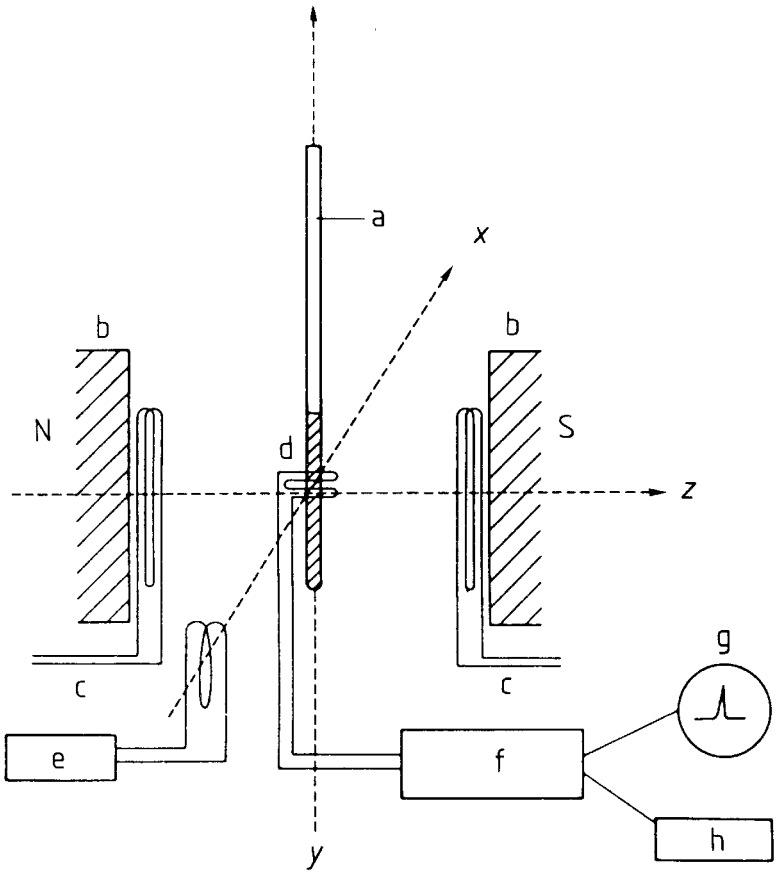

Scheme of a continuous wave NMR-spectrometer: a sample, b magnet, c sweep coils, d receiver, e sender, f amplifier, g oscilloscope, h digitizer and computer. In principle, a Fourier transform NMR spectrometer operates similarly, but the sender e is substituted by an impuls generator and f by an array of complex electronic devices.

Figure 6.6 Scheme of a nuclear magnetic resonance spectrometer.

Figure 6.6 shows a scheme of a typical continuous wave NMR spectrometer. The instruments are often named after their operating frequency (e.g. a 500 MHz NMR spectrometer). Modern NMR spectrometer use Fourier transform techniques instead of the older continuous wave operation.

6.2. Structure of an NMR-spectrum

Each NMR spectrum is characterized primarily by two properties. The chemical shift determines how much the absorption line is shifted due to magnetic shielding by the chemical environment of the absorbing nucleus. The chemical shift therefore characterizes the position of the absorption peak relative to an unshielded nucleus. The second property that determines the appearance of an absorption line is the spin-spin coupling, which leads to a multiplet structure of the NMR spectrum. The spin-spin coupling is caused by a magnetic interaction between nuclei in close proximity to each other. The chemical shift and the spin-spin coupling will be observed independent of the nucleus, i.e. these properties are found for ^{1}H, ^{13}C, ^{15}N, etc. The differences between the nuclei are in the different positions of the resonance lines. For instance if the B_0-field is 10 T, the ^{1}H resonance appears at 425.7 MHz, and the ^{13}C resonance at 107.1 MHz. With one experiment (B_0-field), only one kind of nucleus can be investigated spectroscopically.

6.2.1 Chemical shift

Until now, we have described the NMR experiment for isolated nuclei. However, this is not very realistic, since all nuclei are associated at least with electrons in an atom or molecule. The B_0-field induces ring currents in the electron cloud in an atom. These ring currents are in turn inducing a magnetic field B_i which is directed against to the B_0-field. The investigated nucleus is shielded and a stronger field B_0 has to be used for nuclear magnetic resonance to take place. The magnitude of the induced field is dependent on the magnitude of the B_0-field. The local field is therefore given by

$$B_{loc} = B_0 - \sigma \cdot B_0 = B_0(1-\sigma) \qquad \text{Eq. 6.16}$$

The shielding constant σ is strongly dependent on the electron density, i.e. also on the neighbor atoms of the nucleus. For example, the electron density close to the proton of a methyl group (CH_3) is much larger than the electron density of a proton in a O-H group, because of the higher electronegativity of the oxygen in OH. Therefore the shielding constant will be larger for the proton in OH than for that in CH_3. Shielding can also be influenced by neighbor groups like (-CH_3, -NH_2,. -COOH, etc).

A special shielding effect is observed in benzene (Figure 6.7). The B0-field induces a ring-current in benzene. In the center of the ring, the induced magnetic field of the molecule is directed against the B0-field, but outside the ring, where the aromatic protons are located, the induced magnetic field has the same direction as the B_0-field. Thus the field at the protons is enhanced and shielding is weakened. The resonance of such protons occurs at relatively small field. The chemical shift is a characteristic quantity that depends on the chemical environment of the nucleus. The importance of NMR as a tool to probe the chemical environment is thus obvious.

For practical reasons, the chemical shift is expressed independently of the magnetic field B_0 and radiation frequency, by a reference signal:

$$\delta = \frac{\nu_{ref} - \nu}{\nu_{ref}} \cdot 10^6 \text{ ppm} \qquad \text{Eq. 6.17}$$

Thus a chemical shift of 300 Hz in a 300 MHz spectrum would have a δ of 1 ppm and a shift of 600 Hz in a 600 MHz spectrum would also be 1 ppm. In ^{1}H-NMR spectroscopy, the reference signal is that of tetramethylsilane (TMS, $Si(CH_3)_4$) in organic solvent or 2,2,-dimethyl-2-silapentan-5-sulfonate (DSS) in aqueous solvent. In comparison to most other protons, the protons in these compounds have a better chemical shielding.

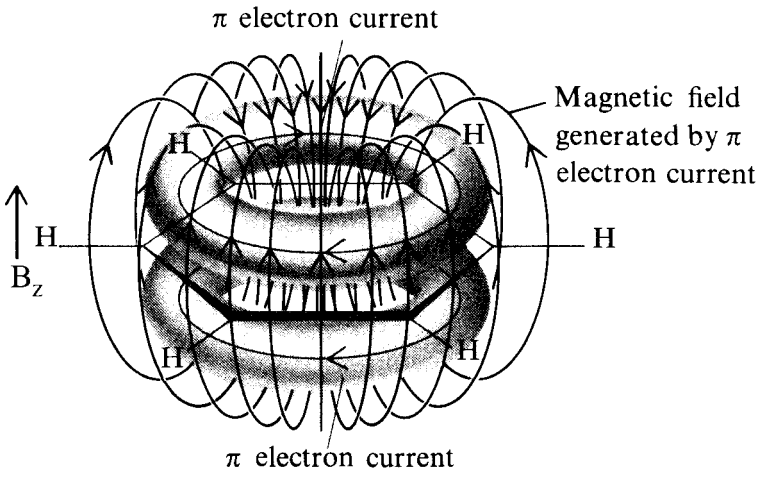

The ring-current effect on the local magnetic field felt by aromatic protons.
The applied external field is B_z.

Figure 6.7 Shielding effect by the π-electrons in benzene.

The chemical shift is given in ppm units from the right to the left in a spectrum. Positive numbers characterize a shift of the resonance line to a lower magnetic field B_0. Some chemical shift values in ^{1}H-NMR are given in Figure 6.8.

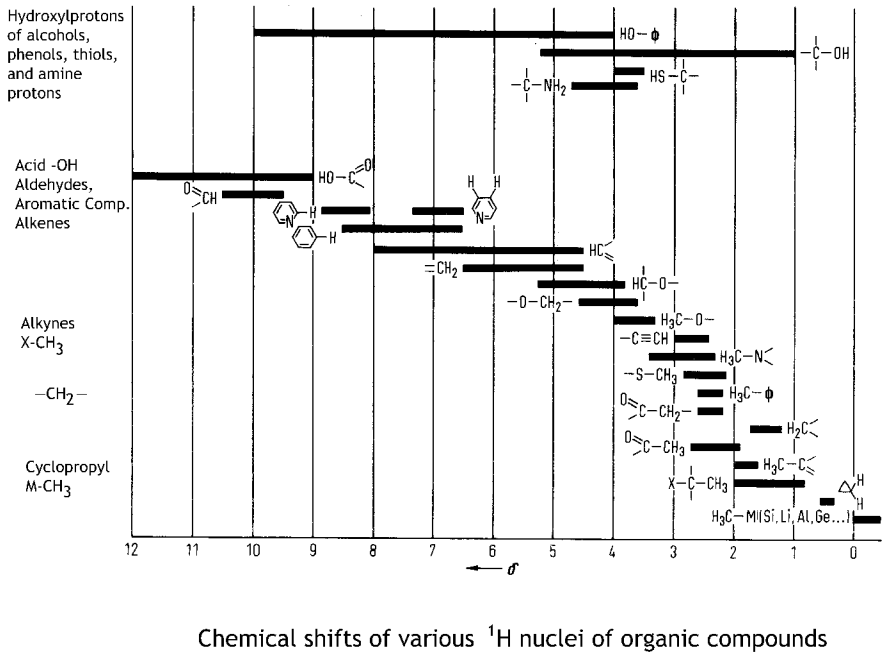

Figure 6.8 Some chemical shift values of proton resonances in ^{1}H-NMR spectra.

6.2.2 Spin-spin coupling.

In Figure 6.9 the proton NMR spectrum of alanine in D_2O is shown at pD=13. At a pD of 13 all amine protons are exchange by deuterium, D. Because of the chemical shift, the doublet at δ=1.21 ppm can be assigned to the methyl protons and the quadruplet at δ=3.31 ppm can be assigned to the α-carbon hydrogen. The appearance of multiple resonance lines is a consequence of the spin-spin coupling between protons in direct neighborhood, because the carbon atoms are mostly present as ^{12}C, which does not have a spin. We observe a vicinal proton-proton coupling. The magnitude of the proton-proton coupling is expressed by the coupling constant J, which is in the region of 0 to 30 Hz for protons in 100 MHz spectra (approx. 0.2 ppm).
How can the coupling be explained ? The 3 protons of the methyl group are magnetically equivalent. Without a spin-spin interaction we would observe one resonance line at 1.21 ppm, because the coupling of equivalent nuclei does not affect the NMR spectrum. The hydrogen at the neighbor α-carbon can be in two different spin states with m_I=–1/2 or m_I = +1/2. The corresponding magnetic moments of these spins lead to a local decrease or increase of the magnetic B_0 field. The NMR signal of the methyl protons is split into a doublet. An equivalent

consideration leads to the quadruplet of the NMR resonance line of the hydrogen at the α-.carbon atom. The spins of the three individual protons can be combined to a total spin that can be either +3/2, +1/2, –1/2, and –3/2. We obtain two different field amplifications and two different field attenuations, therefore, 4 resonance lines. From this and similar considerations

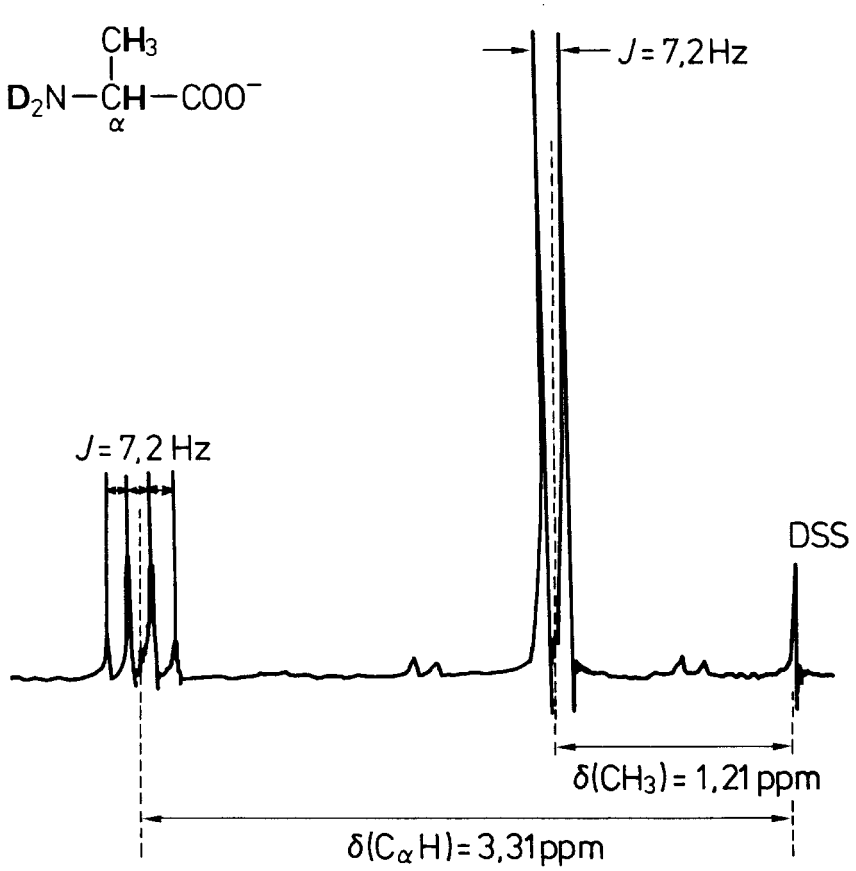

^{1}H-NMR spectrum of alanine

Figure 6.9 Proton NMR spectrum of alanine

we can derive the general rule that n equivalent nuclei with spin 1/2 in direct neighborhood of a proton lead to n+1 multiplet components in the NMR spectrum of this proton. The intensities of these peaks can be derived from Pascals triangle:

n=0			1			
n=1		1		1		
n=2		1	2	1		
n=3	1	3	3	1		
n=4	1	4	6	4	1	

In case of the C-α hydrogen, the observed intensities of individual bands in the multiplet are 1:3:3:1. Multiplets with superpositions arise from couplings with more than one set of nuclei. In Figure 6.10 this is shown on the example of the amino acid lysine.

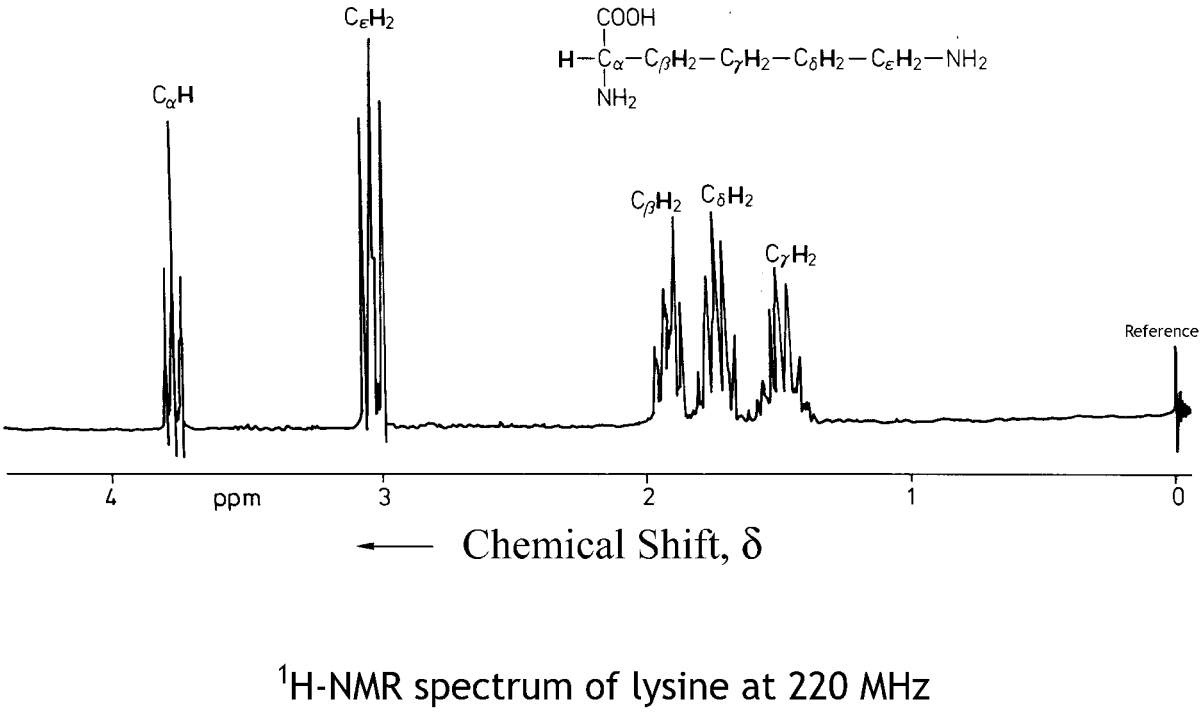

^{1}H-NMR spectrum of lysine at 220 MHz

Figure 6.10 Proton NMR spectrum of lysine at 220 MHz.

The scalar coupling that has been observed in the two examples of alanine and lysine is also called J-coupling or indirect coupling, because it is mediated by the bonds between the nuclei. Direct coupling or through-space coupling is also observed, but mostly in the solid phase. In liquids, the direct coupling is often averaged to zero because of the fast rotational motion of the molecules.

The scalar coupling constant is given by the splitting of a resonance line and given in the frequency unit Hertz (Hz). Different type of scalar coupling are distinguished. The scalar coupling constant of two nuclei that are separated by N bonds is denoted ^NJ, with subscripts of the type of nuclei involved. Thus, $^1J_{CH}$ is the coupling of a proton directly joined to a ^{13}C atom. $^2J_{CH}$ is the coupling constant when the same nuclei are separated by 2 bonds, such as in ^{13}C-C-H. A typical value of $^1J_{CH}$ is in the range of 120 to 250 Hz. The coupling constant is a consequence of the nuclear magnetic moment and therefore independent of the external B0 field. Therefore the coupling constant is given in Hz. $^2J_{CH}$ is between 0 and 10 Hz. Both 3J and 4J give detectable effects in a spectrum, but couplings over larger numbers of bonds can generally be ignored. The sign of the coupling indicates whether the energy of the two spins is lower when they are parallel or when they are antiparallel. Spin-spin coupling in molecules in solution can be explained in terms of the polarization mechanism, in which the interaction

is transmitted through the bonds. The simplest case is to consider $^1J_{XY}$ where X and Y are spin 1/2 nuclei joined by an electron pair bond. The coupling mechanism depends on the fact that in some atoms it is favorable for the nucleus and a nearby electron spin to be both parallel (both α or both β), but in others it is favorable for them to be antiparallel (one α, one β). The electron-nucleus interaction is magnetic in origin, and may be either a dipolar interaction between the magnetic moments of the electron and nuclear spins or a Fermi contact interaction. The Fermi contact interaction depends on the very close approach of the electron to the nucleus and can occur only if the electron occupies an s orbital. The Fermi

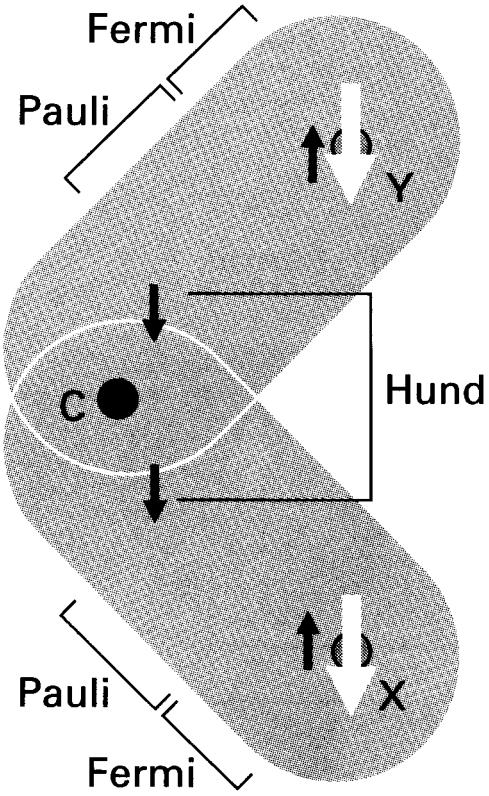

The polarization mechanism for $^2J_{HH}$ spin–spin coupling. The spin information is transmitted from one bond to the next by a version of the mechanism that accounts for the lower energy of electrons with parallel spins in different atomic orbitals (Hund's rule of maximum multiplicity). In this case, J is negative, corresponding to a lower energy when the nuclear spins are parallel.

Figure 6.11 Indirect spin-spin coupling mechanism between geminal hydrogens.

contact interaction is a consequence of the different magnetic field pattern that is present close to the nucleus. It is usually energetically favorable for a nucleus and an electron to be antiparallel. If the x nucleus is an α, a β electron of the bonding pair will tend to be found nearby (since that is energetically favorable for it). The second electron in the bond, which must have an α-spin if the other is β, will be found mainly at the far end of the bond because electrons tend to stay apart from each other. Because it is energetically favorable for the spin of Y to be antiparallel to an electron spin, a Y nucleus with a β-spin has a lower energy and hence a lower Larmor frequency than a Y nucleus with an α spin. The opposite is true for an X with β, for now the α -spin of Y has the lower energy. In other words, the antiparallel arrangement of nuclear spins lies lower in energy as the parallel arrangement as a result of their magnetic coupling with the bond electrons. That is $^{1}J_{HH}$ is positive. To account for the value of $^{2}J_{XY}$, as in HCH, we need a mechanism that can transmit the spin alignments through the central C-atom, which may be ^{12}C with no nuclear spin of its own. An X-nucleus with an α-spin polarizes the electrons in its bond and the α-electron will be found closer to the C-nucleus. The more favorable arrangement of two electrons on the same atom is with their spins parallel (Hunds rule). So the more favorable arrangement is that of the electron with the α-spin to be near the C-nucleus. Consequently, the β-electron will be closer to the Y-nucleus, which in turn will have a lower energy if it has an α spin, i.e. its spin will be parallel to that of the X-nucleus and the coupling constant will be negative.

The coupling of a nuclear spin to an electron spin by the Fermi contact interaction is most important for proton spins, but is not necessarily the most important mechanism for other nuclei. These nuclei may also interact by a dipolar mechanism with the electron magnetic moments and with their orbital motion, and there is no simple way of specifying whether J will be positive or negative.

The vicinal H,H coupling , ^{3}J(H,H), has been well investigated, since it is found in saturated hydrocarbons. It was found that the coupling is dependent on several factors:

- the torsion angle
- the substituents
- the C-C distance
- the H-C-C- valence angle

As an example the dependence of the ^{3}J(H,H) coupling on the torsion angle is depicted in Figure 6.12. The coupling as a function of the torsion angle is described by the Karplus equation:

$$J = A + B\cos(\phi) + C\cos(2\phi) \qquad \text{Eq. 6.18}$$

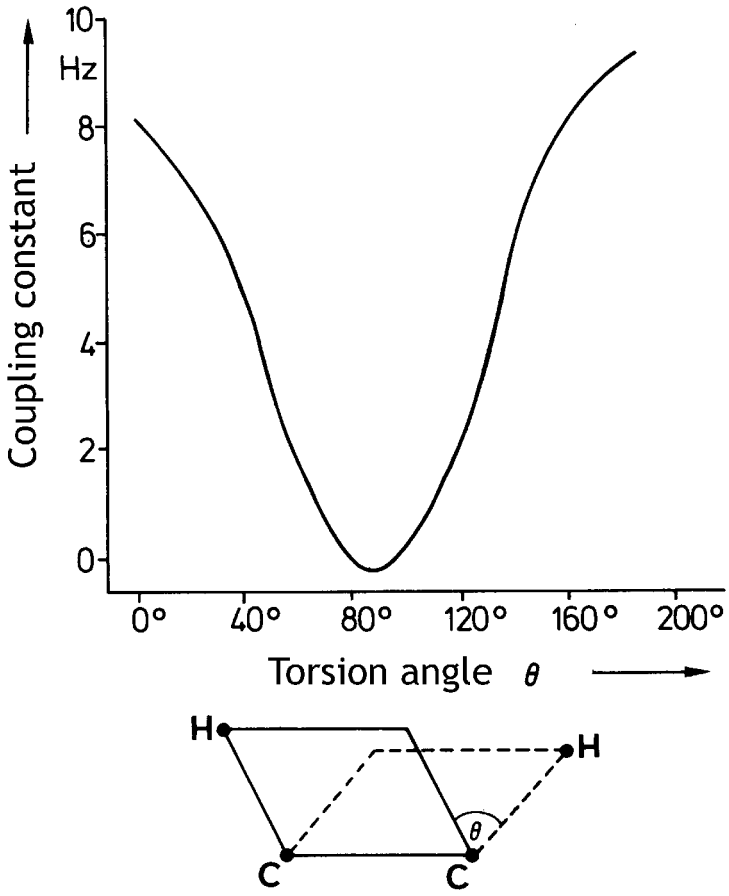

Dependence of the coupling constant on the torsion angle between two hydrogen atoms.

Figure 6.12 Dependence of the vicinal 3J(H,H) coupling on the torsion angle.

in which A ≈ +7 Hz, B ≈ –1Hz, C ≈ +5Hz, respectively.

It has already been mentioned that magnetically equivalent protons do not couple among each other. To describe the coupling between magnetically distinct nuclei a nomenclature was introduced in which nuclei with very distinct chemical shifts are described by letters A and X. Nuclei with chemical shifts close to each other are described by letters A and B. We shall first consider an AX spin system, in which both nuclei have the spin 1/2. Suppose the spin of X is α; then the spin of A will have a Larmor frequency as a combined effect of the external field, the shielding constant and the spin-spin interaction with X. The spin-spin coupling will

result in one line in the spectrum of A that is being shifted from A by -1/2 J from the frequency it would have in the absence of coupling. If the spin of X is β, the spin of A will have a Larmor frequency shifted by +1/2 J. Therefore, instead of a single line from A, we get a doublet of lines separated by J and centered on the chemical shift characteristic of A. The same splitting occurs in the X-resonance. Instead of a single line, the resonance is a doublet with splitting J (the same value as in the splitting of A) centered on the chemical shift characteristic of X. A subtle point is that the X-resonance in an AX_n spin-system (such as an AX_2 or an AX_3 species) is also a doublet with splitting J. A group of equivalent nuclei resonates like a single nucleus. The only difference is that the peak intensity is n times higher in an AX_n spin system than in an AX spin system. The A resonance in an AX_n system is quite different from the X resonance in an AX system. In an AX_2 spin system, for example three resonance lines are observed because the two X spins can be either all α, αβ, or all β.

An example for an AX_3 spin system was the spectrum of alanine in D2O/NaOD (Figure 6.9), in which the a-carbon hydrogen resonance is a quadruplet and the resonance of the methyl protons is split into a doublet.

In order to classify a spin system, it is first important to determine the chemically different nuclei and for that purpose the stereo chemistry of the nuclei must be analyzed. In ^{1}H-NMR spectroscopy, homotopic protons are chemically equivalent and give rise to one signal in an isolated group. Enantiotopic protons, for example those in bromochloromethane, are stereochemically not equivalent, but magnetically equivalent, they cannot be distinguished in an NMR spectrum. However, the protons of diastereotopic compounds, for example those in the two methyl groups of valine (Figure 6.13), have a different chemical environment (there is no symmetry operation or bond rotation that could convert these protons into each other.

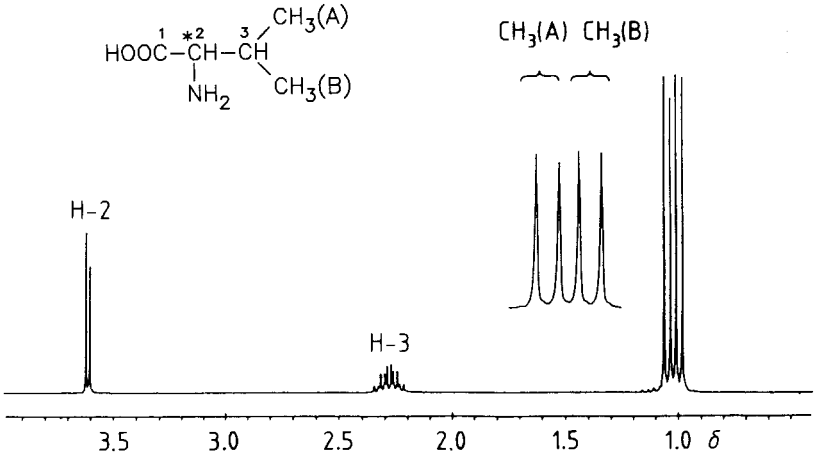

^{1}H-NMR spectrum of valine. The C_α carbon atom is asymmetric. Thus, the two methyl groups on C_β are diastereotropic and give different resonance signals at different chemical shifts. Two dublets are observed because of their different coupling with the C_β-proton.

Figure 6.13 1H-NMR spectrum of valine.

6.3. Examples of ^{1}H NMR spectra of aromatic compounds.

As discussed before, aromatic hydrogen atoms show characteristic chemical shift of about δ = 6.5 to 8.5 ppm. Figure 6.14 shows the spectrum of phenylethane. The aromatic protons exhibit a chemical shift of 7.2 ppm while the methylene protons appear at $\delta \approx 2.6$ ppm and the methyl protons appear at $\delta \approx 1.2$ ppm. The methyl protons appear as a triplet and the methylene protons appear as a quadruplet due to spin-spin coupling.

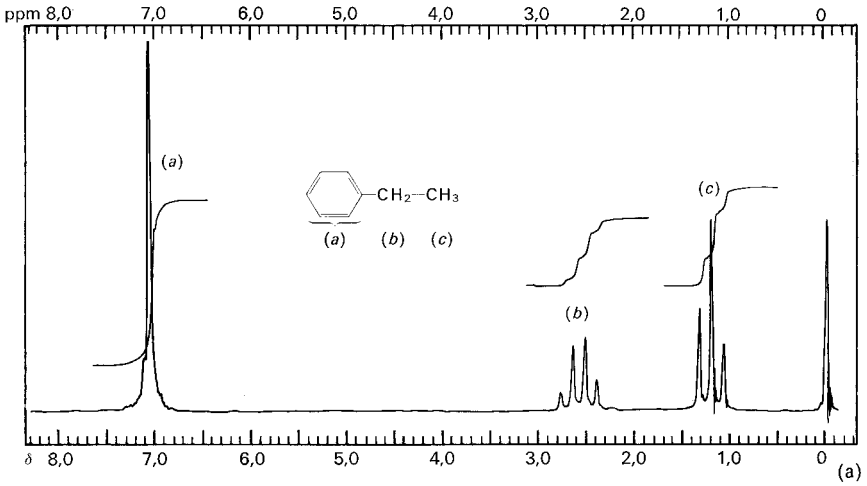

^{1}H-NMR spectrum of ethylbenzene. The triplet of the methyl protons (c), the quadruplet of the methylene protons (b) and the peak of the aromatic protons (a) are observed in the direction of increased chemical shift.

Figure 6.14 ^{1}H-NMR spectrum of phenylethane

The spectrum of Figure 6.14 was obtained at relatively low frequency and is not very well resolved. Thus the differences among the aromatic protons are not very well resolved and only a single peak appears in the spectrum. On a better NMR spectrometer, differences between aromatic protons can be observed and we shall discuss two examples.

In anilline the aromatic protons H2 and H6, H3 and H5 and H6 are different as is evident from the electron densities in the aromatic ring (Figure 6.15). Because of the +M effect of the amino group the electron density is higher at carbon atoms 2,4, and 6 than at carbon atoms 3 and 5. The magnetic shielding of H4 is therefore different from that of H2 and H6. The resonances of H3 and H5 have the lowest chemical shift. The splitting of the resonance lines is complex. The resonance lines of the magnetically equivalent H2 and H6 are split by a J-coupling with the other aromatic protons, and largely appear as a doublet, since the coupling between H2 and H3 (or H5 and H4) is strongest. The resonance line of H4 is split most effectively by the magnetically equivalent protons H3 and H5 into a triplet although there is fine structure by J-coupling over more than 3 bonds. The coarse structure of the resonances

of H3 and H5 may also be described as a triplet. However the protons H2 and H4 that strongly couple with H3 are not magnetically equivalent. Overall the splittings of the aromatic resonances are far more difficult to interpret than those of relatively isolated methyl or methylene groups in phenylethane.

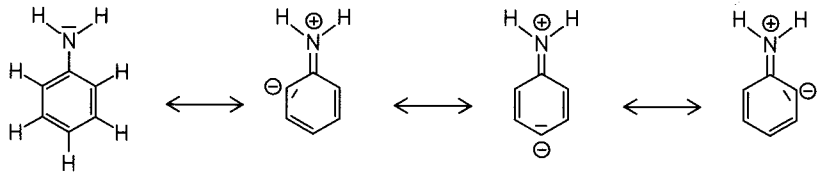

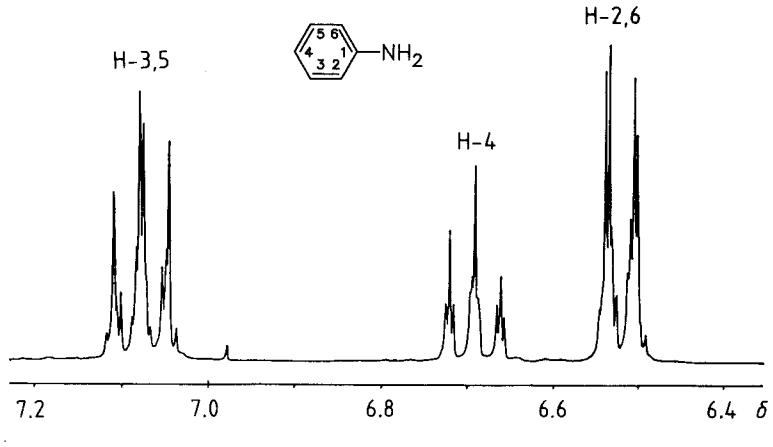

Figure 6.15 250 MHz ^{1}H-NMR spectrum of anilline in $CDCl_3$ ($\delta(NH_2)$ = 3.45 ppm)

Another example of the chemical shift of aromatic protons is given in Figure 6.16 . In nitrobenzene, the nitro group has a -M effect. Thus, the electron density is lower at hydrogens 2, 4 and 6 than it is at hydrogens 3 and 5. Hydrogens 3 and 5 are better shielded and their resonances appear at lower chemical shifts than those of H2, H4, and H6.

Overall the chemical shifts are larger than in the previous sample of anilline, because of the stronger deshielding of the aromatic protons by the nitrogen substituent.

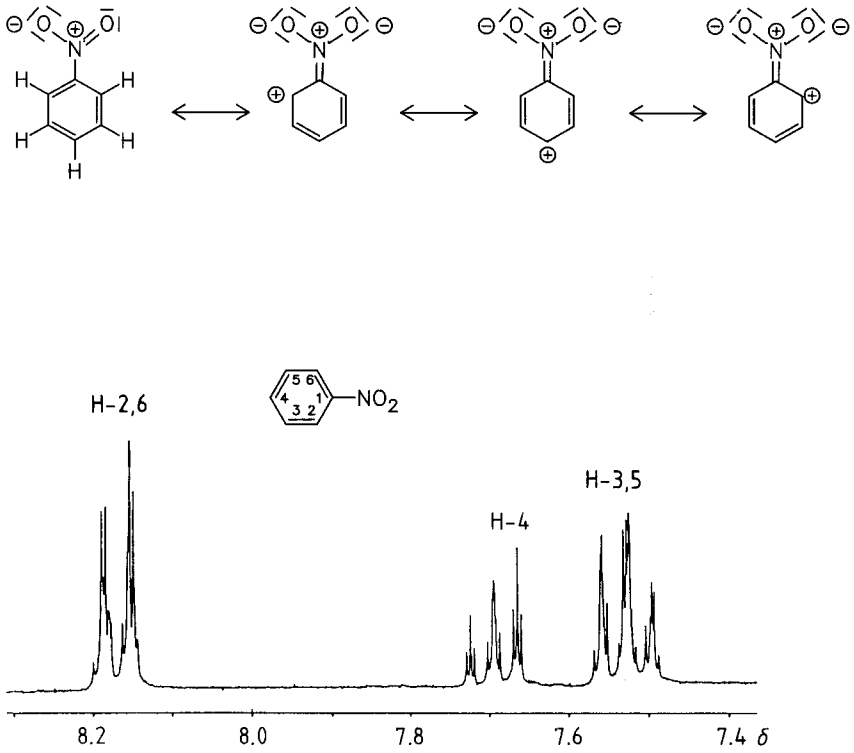

Figure 6.16 250 MHz ^{1}H-NMR spectrum of nitrobenzene in $CDCl_3$.

Numerous experiments with benzene derivatives have shown that the substituents contribute nearly invariably constant changes to the chemical shifts of aromatic protons. These contributions to the chemical shift have been determined from experimental data. With their help and the chemical shift value for the protons of benzene (7.27) it is possible to assign the chemical shifts of many aromatic protons of benzene derivatives.

$$\delta(H) = 7.27 + \sum S \qquad \text{Eq. 6.19}$$

The substituents increments are given for some substituents in the Table 2 below:

Example: p-nitroanisole

δ (H-2, 6)=7.27+So (OCH3) + Sm(NO2)
=7.27–0.43 +0.17 = 7.01 (found: 6.88)

δ (H-3, 5)=7.27+So (NO2) + Sm(O-CH3)
=7.27+0.95 -0.09 = 8.13 (found: 8.15)

in addition δ (OCH3) = 3.90

	ortho	meta	para
Methyl–	–0.17	–0.09	–0.18
Ethyl–	–0.15	–0.06	–0.18
Fluoro–	–0.30	–0.02	–0.18
HO–	–0.50	–0.14	–0.4
–O-CH3	–0.43	–0.09	–0.37
–OCOCH3	–0.21	–0.02	–0.0
–NH2	–0.75	–0.24	–0.63
–N(CH3)2	–0.60	–0.10	–0.62
–CHO	+0.58	+0.21	+0.27
–COCH3	+0.64	+0.09	+0.3
–COOCH3	+0.74	+0.07	+0.20
–NO2	+0.95	+0.17	+0.33

Table 2 Contributions of different substituents to the chemical shifts of aromatic protons.

6.4. Coalescence of spin-spin coupling

The NMR signals are dependent on the possibility of exchange of nuclei. In dimethyl formamide for example, the NMR spectrum consists of two signals of methyl protons that are observed at δ = 2.79 ppm and at δ = 2.94 ppm at 22.5 °C. These two signals are broadened above +100 °C and coalesce at +120 °C to one broad band (Figure 6.17). Upon further temperature increase, this band becomes sharper and positioned in the center of the original peaks. From the temperature dependence of the ^{1}H resonances it is found that the methyl groups are differently shielded at room temperature. The difference is caused by a restricted rotational mobility of the C-N bond, that contains a significant contribution of p-electrons from the nitrogen, leading to a partial double bond character of the C-N bond. At higher temperature (energy), rotation around the C-N bond is possible and the methyl groups become equivalent. The temperature at which the exchange between the nuclei of different chemical shifts becomes possible is called the coalescence temperature.

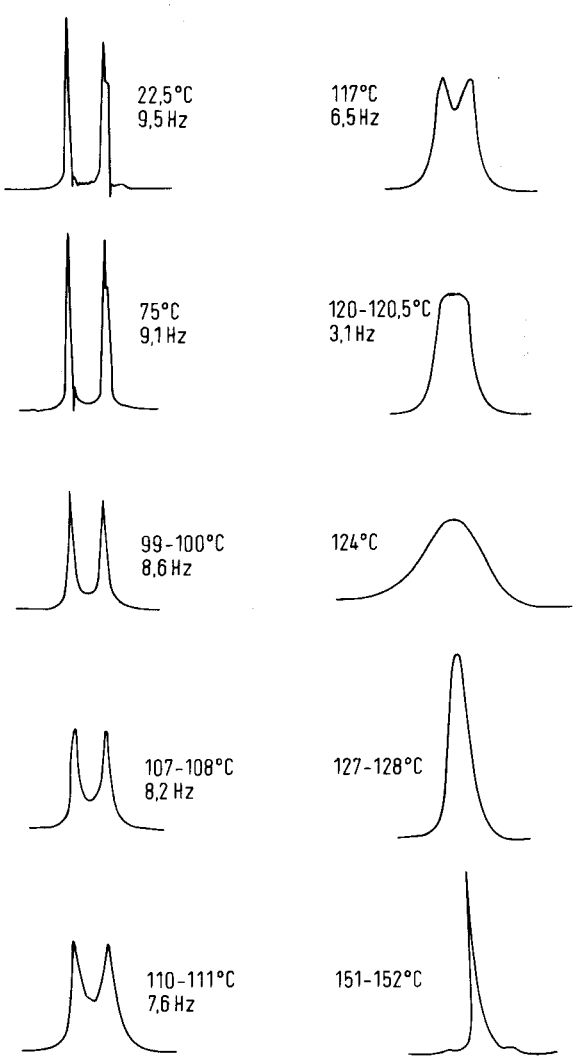

^{1}H-NMR signals of the methyl groups in dimethyl formamide, recorded at different temperatures (frequency: 56.4 MHz). At slow exchange, two signals are obtained, at fast exchange only one signal. In the intermediate region, the signals are broadened. The coalescence temperature is 120 °C.

Figure 6.17 Coalescence of NMR signals.

6.5.Spin-Spin-decoupling and broad-band (BB) decoupling

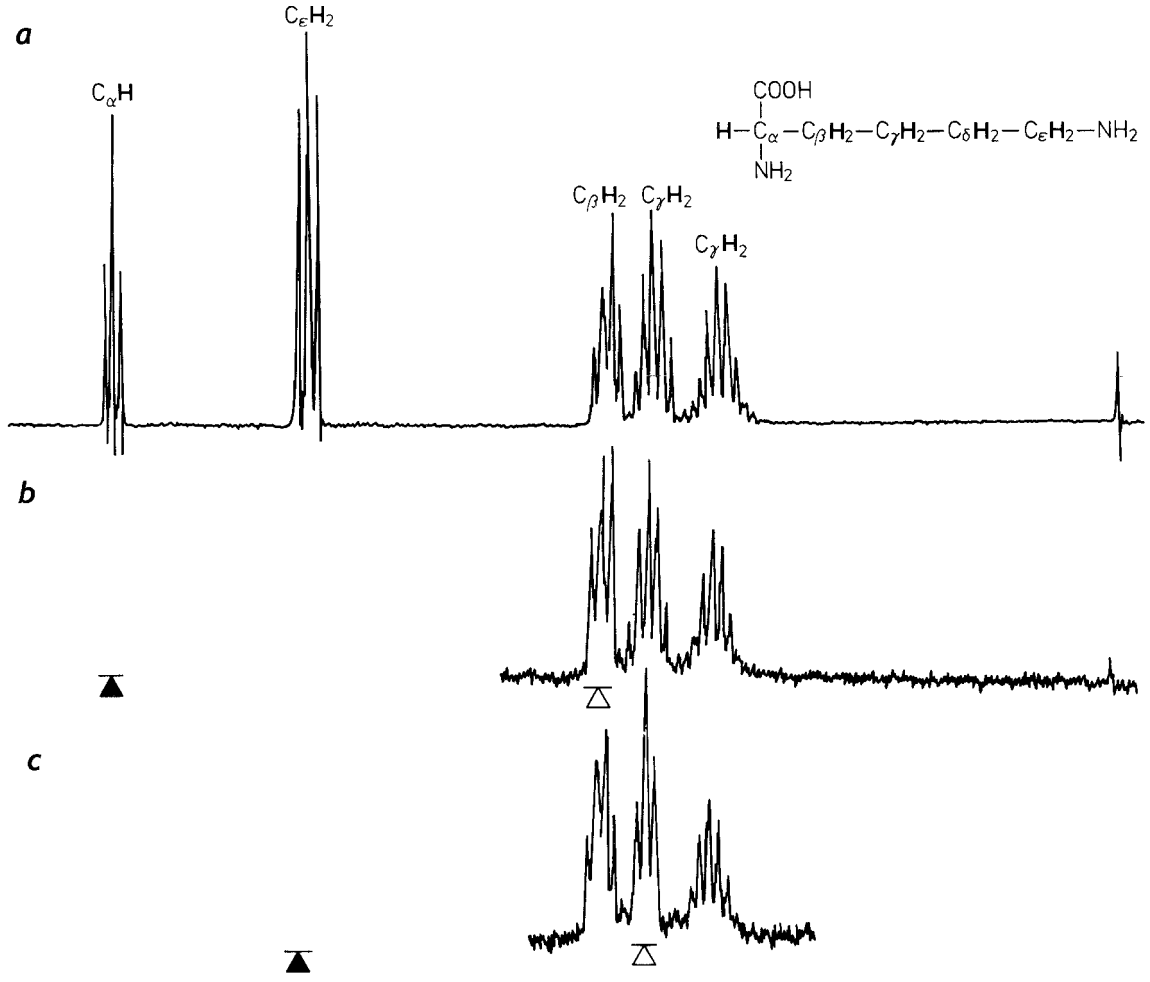

Spin-spin decoupling on the example of lysine in D_2O. ***a*** not decoupled. ***b*** decoupling of the C_α protons. ***c*** decoupling of the C_δ protons. The frequencies of decoupling are indicated by the black arrows. The white arrows indicate changes in the multiplicities that are observed in when neighbor protons are decoupled.

Figure 6.18 Spin-Spin decoupling of the lysine NMR peaks.

The spin-spin coupling between two chemically distinct spins may be eliminated if the transition of one of these spins is saturated by irradiating the sample with the resonance frequency of this spin. Now the ground state and the excited state of this spin are equally populated and *there are continuously transitions between these states.* Now, this nucleus does not longer contribute to the local magnetic field at the neighbor nucleus, such that the signal of the neighbor nucleus is now not split. For this method, a second sender (decoupler) is necessary, which irradiates the nuclei that are to be decoupled. Figure 6.18 displays the spectrum of lysine with decoupling of the C_α (b) and the C_ε protons (C). Changes in the spectrum are marked by arrows. Similarly, in ^{13}C-NMR spectra, all ^1H couplings may be "broad-band decoupled" by irradiating with a "white" frequency spectrum in the region of the

proton resonances.

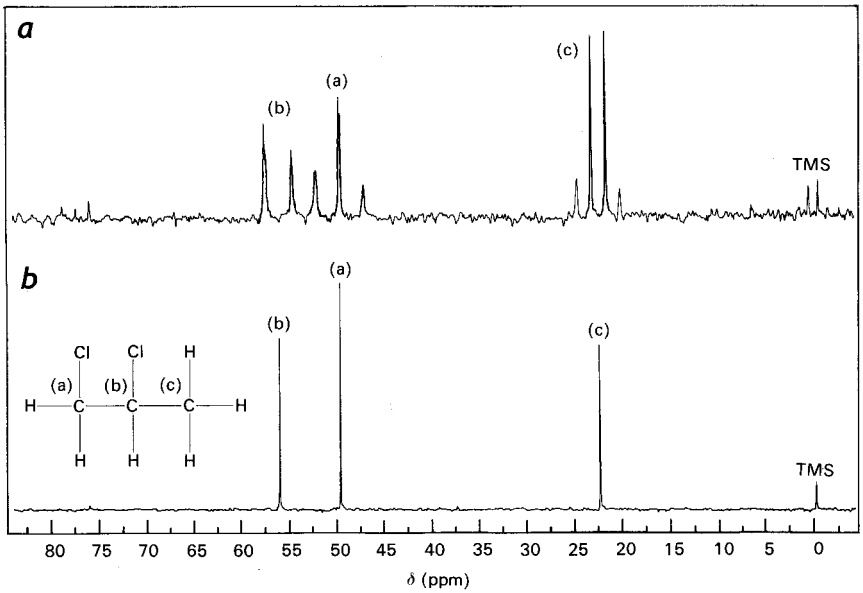

a ^{13}C-NMR spectrum of 1,2-dichloropropane. *b* Proton-decoupled ^{13}C-NMR spectrum of 1,2-dichloropropane.

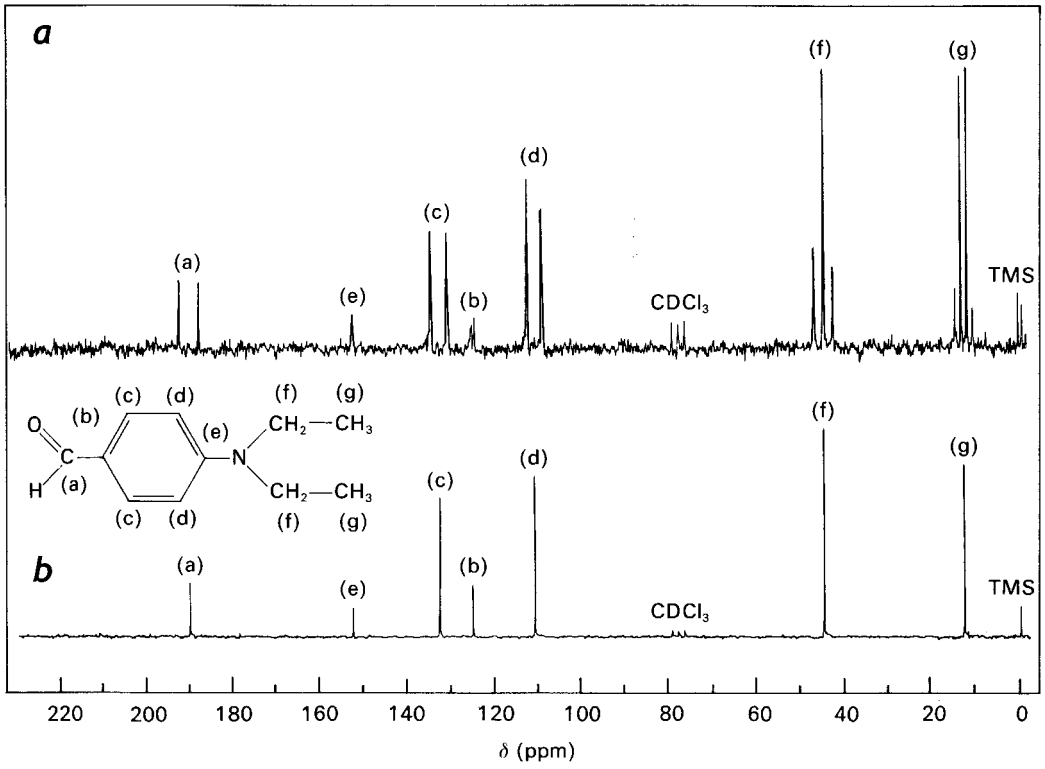

a ^{13}C-NMR spectrum of p-diethylaminobenzaldehyd (in $CDCl_3$).
b Proton decoupled ^{13}C-NMR spectrum of p-diethylaminobenzaldehyd (in $CDCl_3$).

Figure 6.19 13C NMR spectra of p-diethylaminobenzaldehyd.

6.6. Resonance frequencies of some nuclei with non-zero spin

Given the resonance condition

$$\Delta E = g_N \beta_N B_0 = h\nu \qquad \text{Eq. 6.20}$$

the frequency at which the nuclear magnetic resonance will occur in a given field B_0, will depend on the properties of the nucleus (or if the electron is considered, on the spin and magnetogyric ratio of the electron). Typical resonance frequencies of various nuclei in a field of B_0=2.3487 T are shown in Table 3.

Nucleus	Spin	Resonance Frequency (MHz) field of 2.3487 T	g-value
^{1}H	1/2	100.00	5.585
^{10}B	3	10.75	0.6002
^{11}B	3/2	32.08	1.792
^{13}C	1/2	25.14	1.404
^{14}N	1	7.22	0.4036
^{15}N	1/2	10.13	–0.5660
^{17}O	5/2	13.56	–0.7572
^{19}F	1/2	94.07	5.255
^{29}Si	1/2	19.87	–1.110
^{31}P	1/2	40.48	2.261
^{35}Cl	3/2	9.8	0.5472
e	1/2	65752.8	2.000323

Table 3 Resonance frequencies of various nuclei.

6.7. Relaxation

6.7.1 Boltzmann distribution of spins in a magnetic field.

Transitions between the different energy levels the nuclei have in an external magnetic field B0 take place in either direction, from the ground state to the excited state or from the excited state to the ground state. For a nucleus with spin I = 1/2, this means the z-component of that spin can change from m_I = +1/2 to m_I = –1/2 or from m_I=–1/2 to m_I = +1/2. However, the number of absorption and emission processes will depend on the number of spins in the

two energy levels, which nuclei with spin 1/2 can occupy in presence of the external field B_0. The Boltzmann distribution describes the relation between the number of spins found in the lower and upper energy levels:

$$\frac{n_h}{n_l} = \exp\left(-\frac{\Delta E}{kT}\right) = \exp\left(-\frac{g_N \beta_N B_0}{kT}\right) = \exp\left(-\frac{g_N \gamma \hbar B_0}{kT}\right) \qquad \text{Eq. 6.21}$$

The magnetogyric ratio $\gamma = \frac{Ze}{2m}$ is specific for a nucleus and thus the ratio of the number of spins in the excited state to the number of spins in the ground state is dependent on the which species of nuclei is investigated. For example in a field of B_0 = 10 Tesla at T=300 K:

1H: Z=1, e=1.6019e–19 As, m=1.67262e-27 kg. $\gamma = \frac{Ze}{2m}$ = 4.7894e7 As/kg, g_N = 5.585

$\frac{n_h}{n_l}$ = 0.999932

13C: Z=6, e=1.6019e–19 As, m=2.1760e-26 kg. $\gamma = \frac{Ze}{2m}$ = 2.20892e7 As/kg, g_N = 1.404

$\frac{n_h}{n_l}$ = 0.999992

e: Z=1, e=1.6019e–19 As, m=9.1095e–31 kg. $\gamma = \frac{Ze}{2m}$ = 8.794e10 As / kg, g_e=2.000232

$\frac{n_h}{n_l}$ = 0.956203

The absorption of radiation is proportional to the difference between the populations of the ground state and the excited state. Thus, the NMR-spectroscopy of the proton is far more sensitive then the NMR spectroscopy of ^{13}C, and NMR methods are far less sensitive than the ESR method.

6.7.2 Relaxation mechanisms.

The difference between the populations of the ground state and the excited state in thermal equilibrium as it is given by the Boltzmann distribution, is changed when radiation is absorbed. This will finally result in that the populations in the excited state and in the ground state will be equally populated and the signal would disappear. This does not happen, because of relaxation mechanisms that lead to the transitions of nuclei in the excited spin state (parallel to the field B_0) to the ground state.

Two mechanisms of relaxation can be distinguished, the spin-lattice relaxation (longitudinal

relaxation) and the spin-spin relaxation (transverse relaxation). We have seen in section 6.1.2 that the transition of the spins that are oriented parallel to the external magnetic field B_0 and therefore result in a macroscopic magnetization in z-direction (field direction), to the exited state takes place by irradiation with polarized radiowaves. Thus a transverse magnetization in the direction of the x-y plane is observed, corresponding to the phase coherence of the precessing spins and an increased number of spins that have antiparallel orientation towards the magnetic field B_0. If the radio wave (field B_1) is turned off, the longitudinal magnetization M_z in the direction of the external field B_0 will be restored after some time, due to molecular motions. And after some other time the phase coherence of the precessing spins will be lost, due to the magnetic dipole-dipole interaction with neighboring molecules. The first relaxation process, the longitudinal or spin-lattice relaxation, is characterized by the longitudinal relaxation time T_1, which is the time after which the fraction 1/e of the excited spins have returned to the ground state or restored the longitudinal magnetization M_z. The second relaxation process is defined by the transverse relaxation time or spin-spin relaxation time, after which the fraction 1/e of the precessing spins has lost its phase coherence (i.e. its transverse magnetization M_{xy}). The spin-spin relaxation affects the lifetime of a spin-state but not the population ratio of the excited and the ground state. The two functions for the return of the magnetization M_z and the decay of the transverse magnetization M_{xy} are shown in Figure 6.20

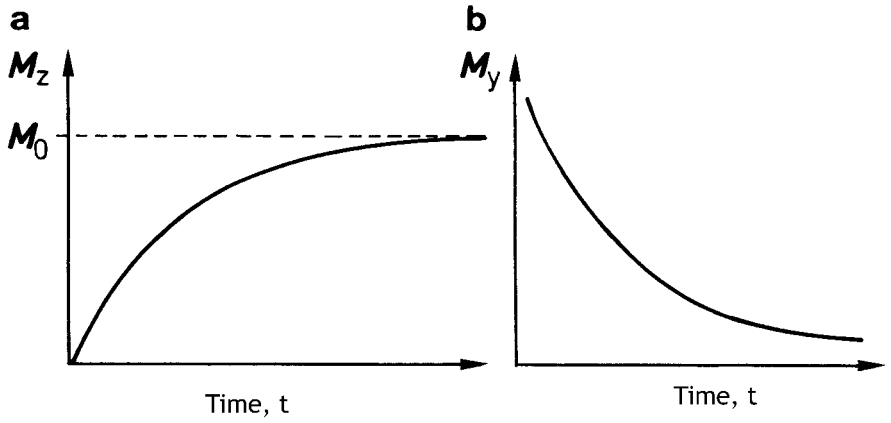

Time dependence of the change in the magnetization after shutting down the B_1-field. *a* longitudinal magnetization, M_Z. *b* transverse magnetization M_y.

Figure 6.20 Return of the magnetization Mz and decay of the magnetization My

and given by the function

$$\frac{dM_z}{dt} = -\frac{1}{T_1}(M_Z - M_{z0}), \qquad \text{Eq. 6.22}$$

integrated $$M_z = M_{z0}\left[1 - \exp\left(-\frac{1}{T_1}\right)\right] \qquad \text{Eq. 6.23}$$

for spin-lattice relaxation and by the functions

$$\frac{dM_x}{dt} = -\frac{1}{T_2}M_x; \frac{dM_y}{dt} = -\frac{1}{T_2}M_y \ ;$$

integrated $$M_{xy} = M_{xy0}\exp\left(-\frac{1}{T_2}\right) \qquad \text{Eq. 6.24}$$

For a given nucleus, the spin-lattice relaxation and the spin-spin relaxation may be either equal in magnitude or quite different. In small molecules in solution or in the fluid phase it is often $T_1 \sim T_2$. In the solid state or in macromolecules in solution it is often $T_1 > T_2$ (the transverse magnetization declines before the equilibrium Boltzmann distribution is reached).
In CW NMR spectroscopy, the effect of B_1 on the magnetization is always compensated by relaxation processes.

6.8. Pulse Fourier Transform NMR

In CW-NMR spectra were recorded upon continuous irradiation of the sample with a field B_1 at a constant frequency and by variation of the external magnetic field B_0. The interpretation of the spectra was characterized by the chemical shift and the spin-spin-coupling constants J.
The NMR spectroscopy was significantly extended by the introduction of the pulse Fourier transform spectroscopy (FT spectroscopy). In pulse Fourier transform spectroscopy, additional information is obtained by determining the two relaxation times.
In the FT-NMR experiment, the B_1 field is generated as a pulse, i.e. it is only switched on for a short moment and the behavior of the spin-system is measured in the time domain. The Fourier transformation is then applied to the time domain spectrum to generate the frequency domain spectrum. The procedure was already described in context with IR spectroscopy and the same principles apply in NMR spectroscopy. A condition is that the short high frequency pulse contains all frequencies from the range of chemical shifts that the investigated nucleus may have. We now have an NMR instrument that will give us spectrum within one second.

By accumulation of spectra with a computer, a better spectrum can be obtained with Fourier transform NMR spectroscopy than with CW- NMR spectroscopy. The gain in intensity is more than a factor 100 for a given accumulation time compared to continuous wave spectroscopy. The Fourier transformation and analysis of the spectra is performed after accumulation of many scans in the time domain.

6.8.1 Pulse technique.

We have described the impact of the field B_1 in Figure 6.4 as a precession of the longitudinal magnetization around the x'-axis of a rotating coordinate system (x',y',z'). The basis of the pulse technique is that a high frequency pulse in the direction of the x' axis with a duration t_p and with a magnetic induction B_1 will cause a rotation of the magnetization M_z in the zy-plane by a defined angle Θ:

$$\Theta = \gamma \cdot B_1 \cdot t_P \qquad \text{Eq. 6.25}$$

The magnetic field B_1 must be chosen such that t_p is small compared to the relaxation times. With typical values of t_p between 1 and 50 µs, it is possible to obtain any angle Θ.

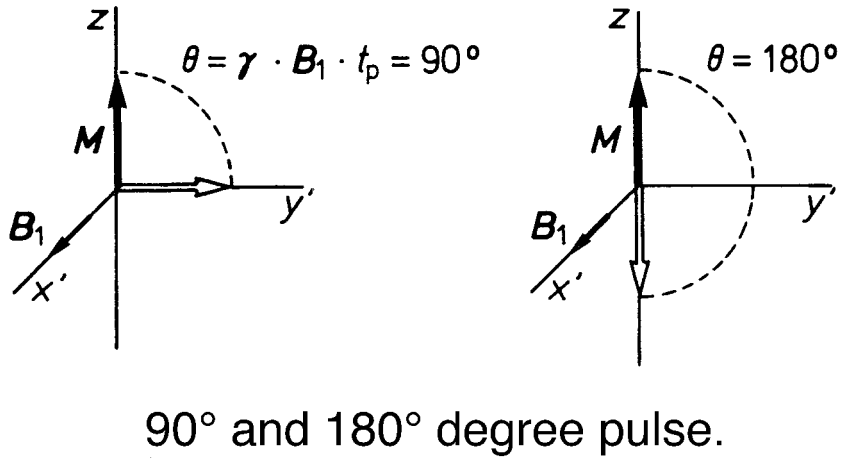

90° and 180° degree pulse.

Figure 6.21 90° and 180 °pulse.

The proportionality constant γ is the magnetogyric ratio that is characteristic for the investigated nucleus. Is the angle Θ by which the magnetization is turned equal 90 ° the pulse is called a 90° pulse, if it is 180 ° the pulse is called a 180 ° pulse (Figure 6.21).

6.8.2 Free induction decay (FID).

The free induction decay (FID) is the decline of the transverse magnetization M_{xy} after a high frequency pulse. For example, we will consider the situation after a 90 ° pulse. The transverse magnetization is maximal in y-direction, and the value of M'_{xy} is the intensity of the NMR

signal. After the B_1 pulse the phase coherence of the spins will decline with the relaxation time T_2:

$$\frac{dM_x}{dt} = -\frac{1}{T_2} M_x ; \frac{dM_y}{dt} = -\frac{1}{T_2} M_y ; \; M_{xy} = M_{xy0} \exp\left(-\frac{1}{T_2}\right) \qquad \text{Eq. 6.26}$$

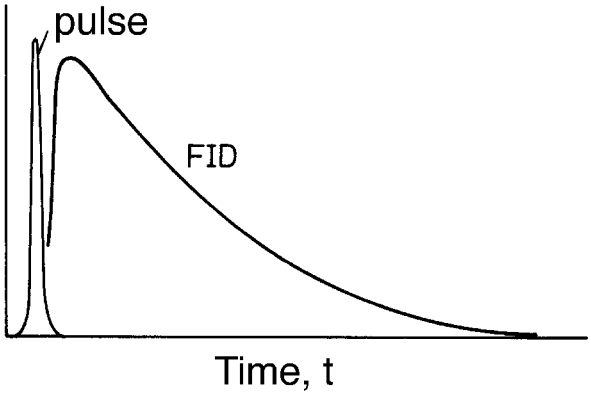

FID after a 90° pulse

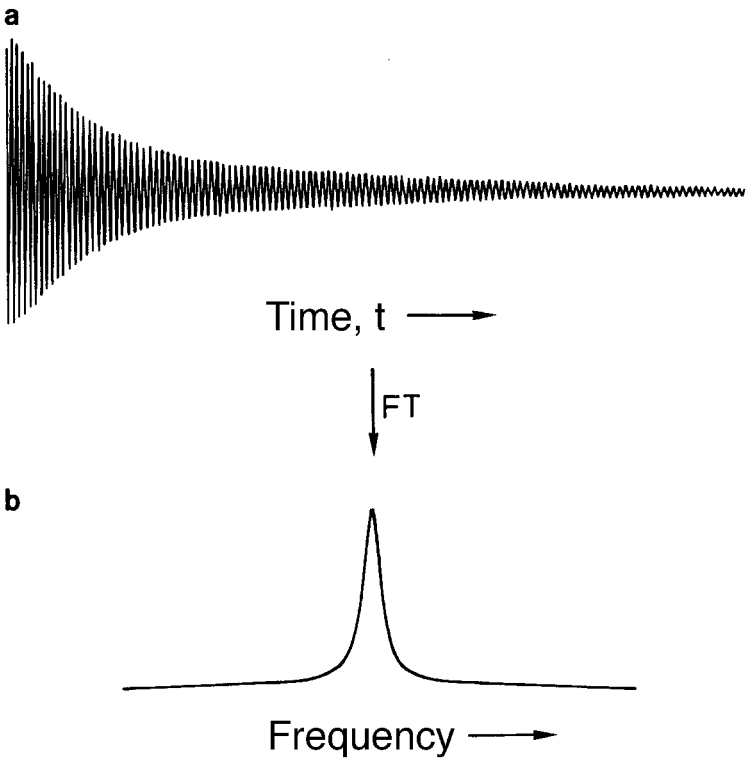

Free induction decay (FID) after a 90° pulse and Fourier transformation.

Figure 6.22 Free induction decay and Fourier transformation after a 90 °pulse.

in an ideal homogeneous magnetic field B_0. In an NMR experiment the field B_0 is not ideal and there are slight inhomogeneities such that the free induction decay is given by

$$\frac{dM_y}{dt} = -\frac{M_y}{T_2^*} \qquad \text{Eq. 6.27}$$

The relaxation time T_2* contains both the contribution of the transverse relaxation and the field inhomogeneities of the magnetic field B_0.

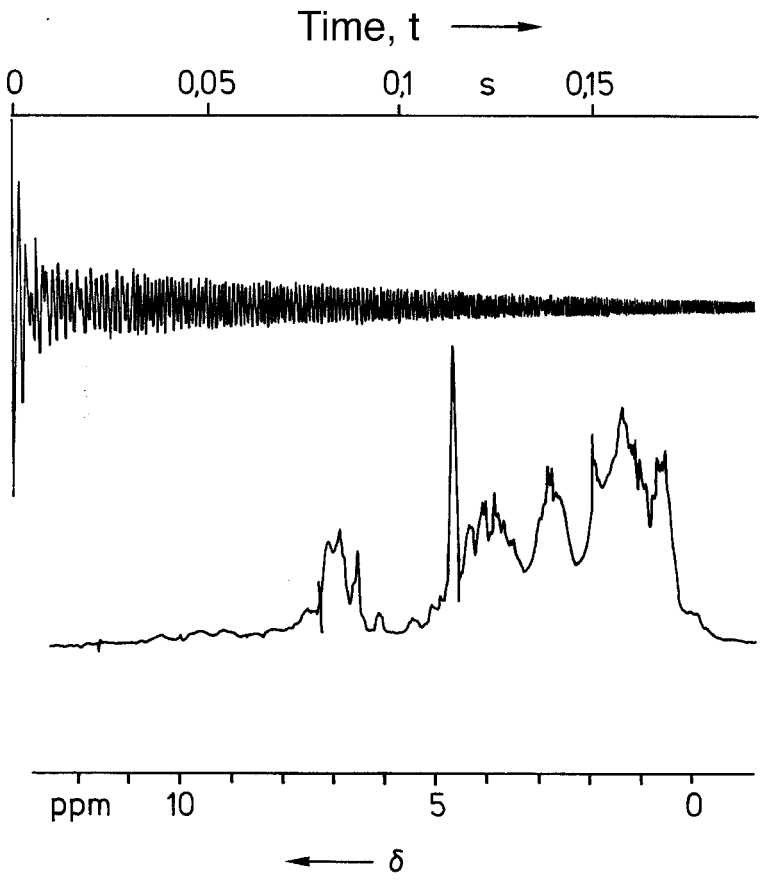

FT ^{1}H-NMR spectrum of basic pancreatic trypsin inhibitor at 100 MHz. 100 FIDs were accumulated after 90° pulses. The spectrum is then obtained by Fourier transformation.

Figure 6.23 ^{1}H NMR time and frequency domain spectra of bovine pancreatic trypsin inhibitor.

The decay function of the transverse magnetization that is depicted in Figure 6.22 is generated only when the pulse frequency is identical to the Larmor frequency of the nucleus, i.e. this function is only observed at one particular chemical shift. The advantage of the FT-NMR is the concurrent observation of the whole spectrum by a high frequency pulse that contains all relevant frequencies. This means that the pulse also contains “off resonance” frequencies.

The resonance frequency and the off resonance frequencies will interfere and the recorded signal will have the line shape of superimposed decaying sine functions. The typical differences between the Larmor and the pulse frequency are approx. 50 Hz. The information that is contained in the time domain in case of resonance and in case of non resonance can be measured and converted from the time domain to the frequency domain by Fourier transform spectroscopy. For protons with different chemical shifts there will always also be the case of non-resonance such that the time domain spectrum is composed of complex superpositions of absorbance signals. After accumulating numerous FIDs, the frequency domain spectrum is calculated (for an example see Figure 6.23).

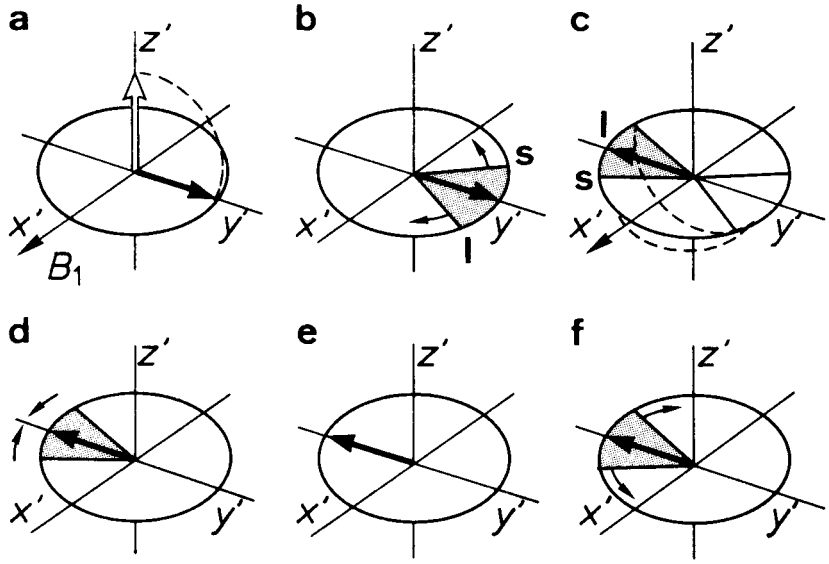

Spin-echo experiment after Hahn. ***a*** A 90° pulse in the direction of the x'-axis changes the magnetization from the z-direction to the y'-direction. ***b*** Due to magnetic field inhomogeneities, some spins are precessing faster (s) than others (l) with respect to the mean value on the y'-axis. The coherence between the spins is lost after some time and M'_y becomes smaller. ***c*** At time t a 180° pulse is performed in x'-direction. The magnetization rotates 180° around the x'-axis. ***d*** After the 180° pulse, the magnetization still precesses in the x'y'-plane, but the l spins are now ahead of the mean-value and the s spins are behind. The phase coherence is re-established, i.e. M'_y increases. ***e*** 2τ after the 180° pulse, all spins are in phase on average. The detected magnetization at t=2τ, the spin-echo, is of the same value as after the 90° pulse and at t>2τ the spins again lose their phase coherence and the process can be repeated.

Figure 6.24 Spin-echo experiment after Hahn to determine the T_2 relaxation time.

6.8.3 Spin-echo method to determine the spin-spin relaxation time T_2.

In a simple experiment, the spin-spin relaxation time can only be measured, if T_2 is small

compared to the contribution of magnetic field inhomogeneities. Otherwise, a value $T_2^* < T_2$ is determined. An experimental method to avoid the problem of field inhomogeneities is the so called spin-echo method by Hahn. This is a multiple pulse method, in which a 90° pulse is followed by a 180 ° pulse after a delay time τ.

In absence of a spin-spin relaxation, the sequence 90°–τ–180° eliminates the different precession frequencies due to magnetic field inhomogeneities. If we consider the spin-spin relaxation, then the transverse magnetization M_{xy} will decline within the time 2τ, because of spin-spin relaxation leading to an equal distribution of the spins on the cone of precession. This effect cannot be avoided by the pulse sequence, such that the spin-echo (M_y'), the signal intensity, is smaller after 2τ and will further decline after every further pulse sequence. From a logarithmic plot of the echo amplitude as a function of the delay time t, the spin-spin relaxation can be determined from a series of 90°–τ–180° pulses (Figure 6.25).

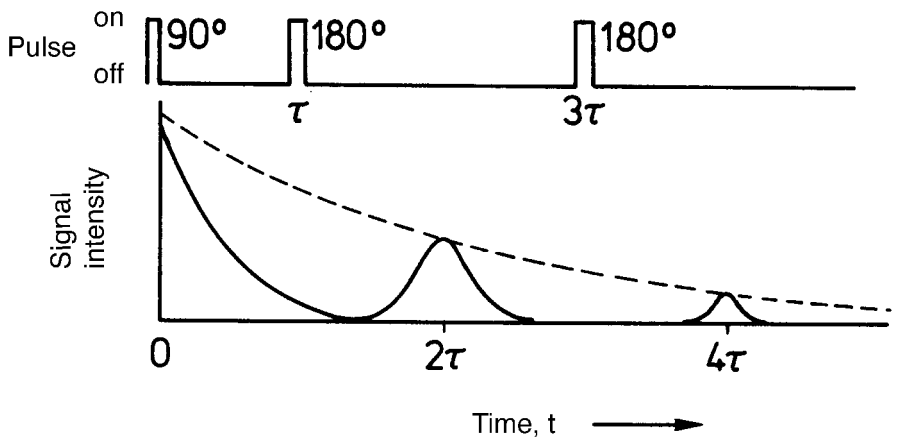

Figure 6.25 Spin-echo intensity as a function of the delay time in a 90°–t–180° pulse sequence.

6.8.4 Determination of T_1.

The spin-lattice relaxation time can also be determined by multiple pulse experiments. Two methods, the progressive saturation and the inversion recovery method shall be described.

6.8.4.1 Progressive saturation.

By 5 to 10 90 ° pulses, a dynamic equilibrium between absorption and relaxation is obtained. After a time τ, the intensity of the NMR signal is measured. If the longitudinal magnetization is not yet fully restored, the intensity of the NMR line will be lower than the maximum value. The intensity of the line (A) will increase with τ up to its maximal value A_∞. A plot of

(A_∞–A) as a function of the delay time will show a linear dependence with a slope of $-1/T_1$ (Figure 6.26).

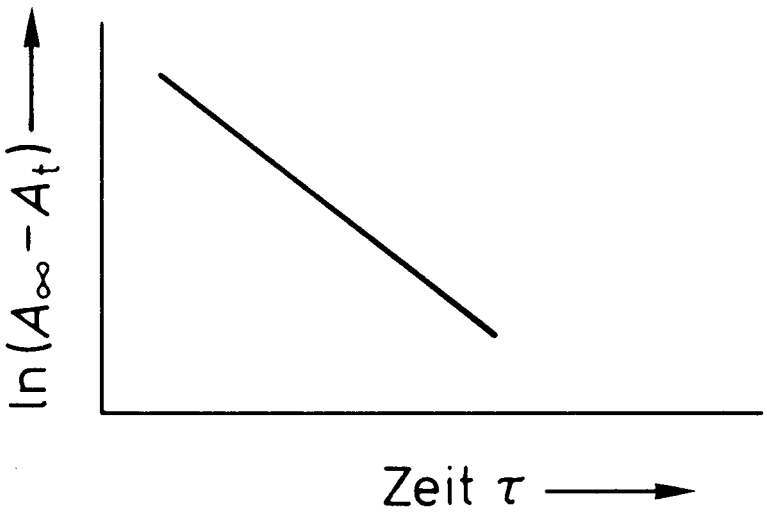

Figure 6.26 Determination of T_1 by progressive saturation. The intensity of the NMR line increases with the time t to its maximum value A_∞.

6.8.4.2 Inversion recovery method.

This method works with a 180°–τ–90°pulse sequence. The 180 ° pulse causes an inverted magnetization in z-direction. After a delay time t, a transverse magnetization is generated by a 90 °pulse and the NMR signal is measured by recording of the free induction decay. With very short times, the magnetization is still pointing to the antiparallel direction and a negative signal is obtained. Only after longer times τ, a positive signal is obtained due to spin-lattice relaxation. In between we observe no signal with $M_z=0$ and $M_y'=0$ at $\tau=T_1$. To obtain T_1, the signal must be recorded as a function of the time τ (up to 100 s). The intensity increases from -A to +A.

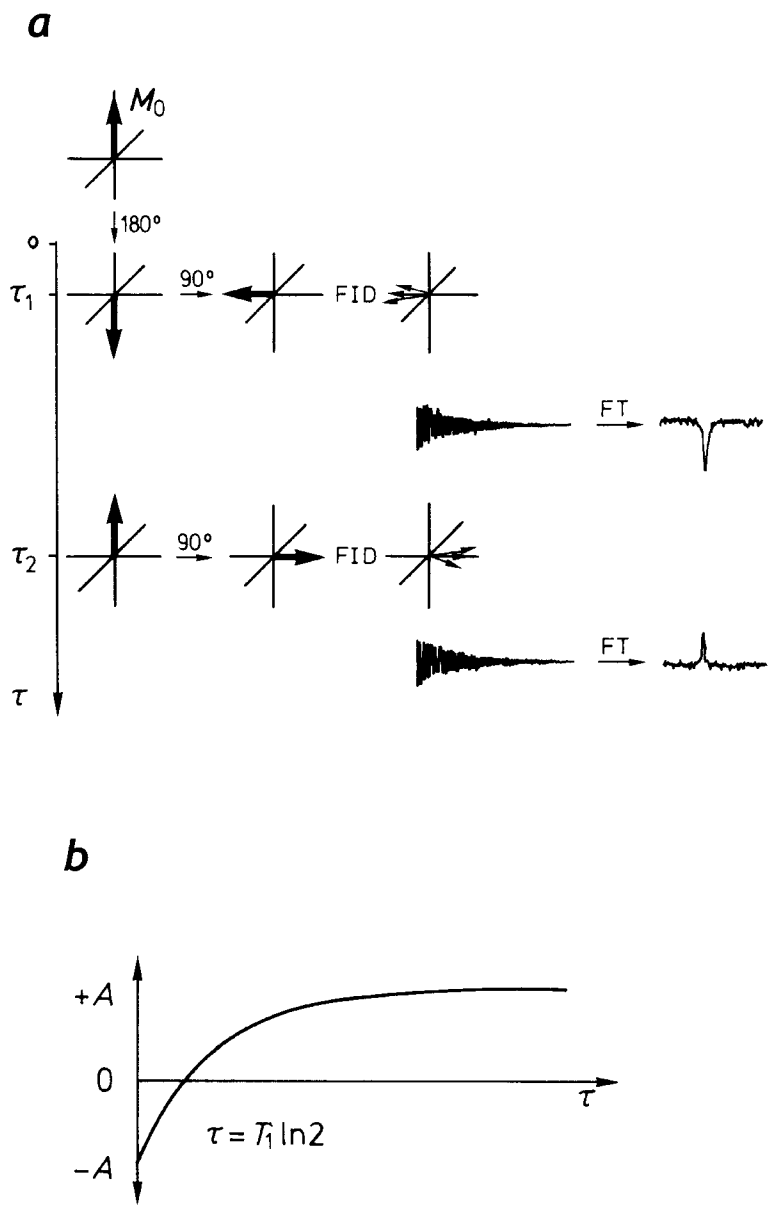

Inversion recovery method to determine the longitudinal relaxation time (spin-lattice relaxation time) T_1 . If the 90° pulse is performed within the time in which M_z is inverted, a negative signal is obtained.

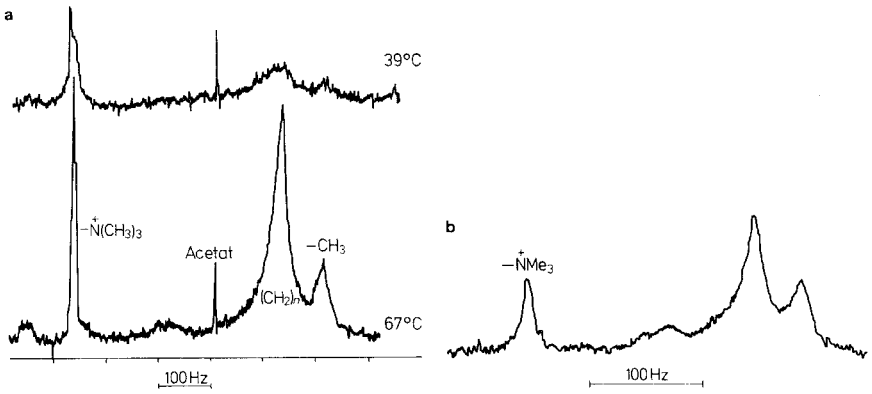

a ^{1}H-NMR spectra of dipalmitoylphosphatidylcholine in aqueous dispersions below and above the phase transition temperature of the lipid.
b ^{1}H-NMR spectrum of vesicles prepared from membranes of the sarcoplasmic reticulum.

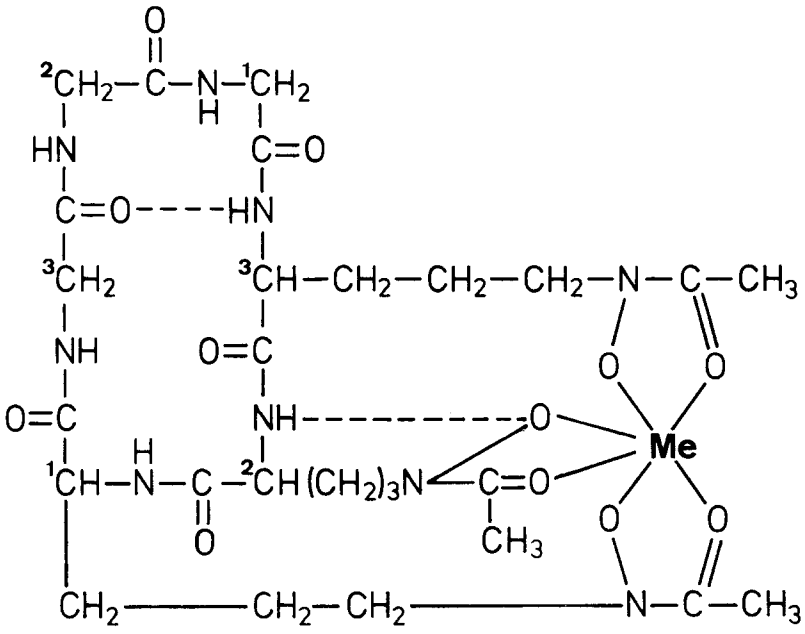

Ferrichrome Iron. The metal ion ion is complexed by a chelate ligand that consists of three glycines and three δ-N-acetyl-δ-N-hydroxyornithines.

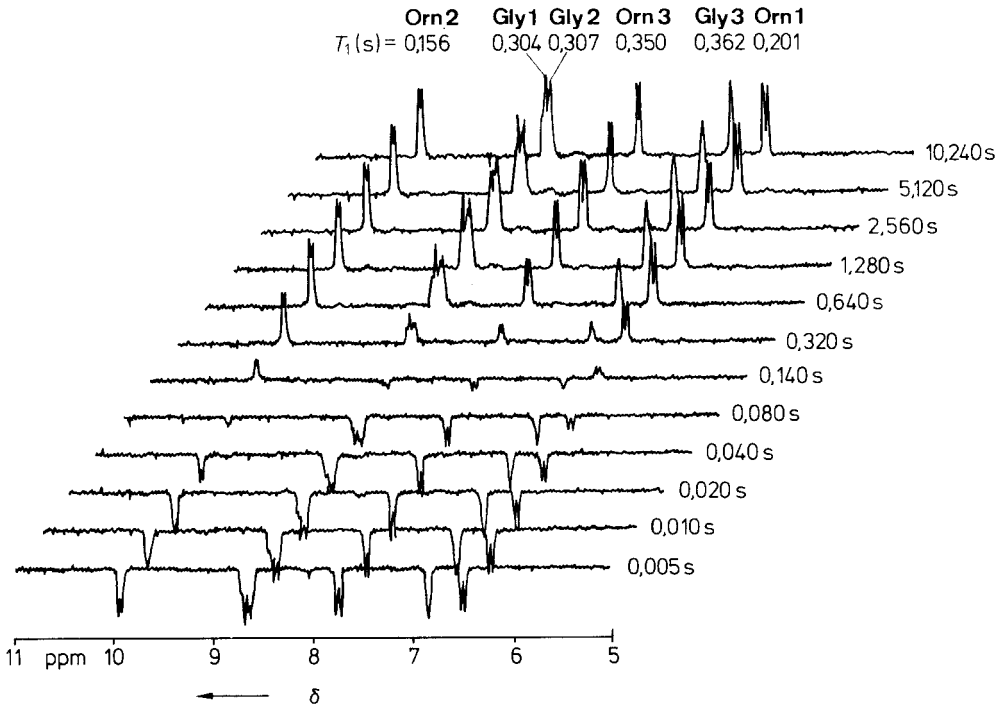

Partially relaxed FT ^{1}H-NMR spectra of the amide protons of Ferrichrome (Al^{3+}) in deuterated DMSO. The delay times after the 180° pulse in a 180°-t-90° pulse sequence are given on the right hand side. The T_1 relaxation times are given at the band assignments.

6.9.NMR Spectroscopy *in vivo*.

In the past 5 decades, the NMR spectroscopy has helped to clarify many chemical and biochemical questions, especially in the investigation of chemical reactions in a test tube. A combined approach of ^{13}C-NMR and ^{1}H-NMR techniques was mostly used. In the last two decades, researchers developed the "in vivo" NMR spectroscopy, the magnetic resonance spectroscopy of living organisms. The NMR techniques then became a valuable tool for biologists and physicians.

Which new insights can be obtained from NMR spectroscopy "in vivo"? How is it possible to obtain information on a large living object, especially given the fact that NMR-spectra of simple molecules are often already very complex ? How is it possible to measure such large samples like humans ?

In "in vivo" NMR experiments, researchers are interested to study chemical reactions in living cells without interferences from outside. The biggest problems that are faced in "in vivo" NMR spectroscopy lie in the magnitude of different molecules and their small concentrations in which they are present in the body. How is it possible to obtain signals and how can these be assigned to defined molecules in the body ?

NMR spectrometers for "in vivo" investigation consist of large magnets which can completely enclose a human body. Technically, the construction of such an NMR spectrometers is solved and these spectrometers are already used in routine experiments. Local NMR experiments at specific body parts are performed with "surface coils", that are adjusted to the surface of the body part under investigation and serve as senders of the high frequency pulse. All other electronic parts are those of a conventional NMR spectrometer. The information that in vivo NMR spectrometers give are chemical shifts and intensities of resonance lines. Only rarely coupling constants are obtained since the resolution of the spectrometer is usually not sufficient to resolve the splitting of the signal.

6.9.1 ^{31}P-NMR spectroscopy *in vivo.*

There are several reasons why the nucleus ^{31}P is suitable for in vivo NMR spectroscopy.

- organic compounds containing phosphorous are key components in the bioenergetics of living organisms.

- the number of different bioorganic compounds that contain phosphorous is limited.

- ^{31}P resonances can be well resolved. ^{31}P nuclei have a large magnetic moment and the natural abundance of ^{31}P is almost 100%. In addition, the concentration of phosphorous is relatively high in many organs, such that one can obtain spectra in a few seconds.

A large part of in vivo applications of NMR methods deal with the investigation of the bioenergetics of the muscle and for medical reasons, investigations of the heart muscle. Investigations of the heart muscle are aggravated because of the motion of the heart. The observation pulses therefore must be triggered to the beat frequency of the heart.
Before we consider a simple example, that of the ^{31}P-NMR spectrum of the forearm, we have to determine which compounds that contain phosphorous are generally found in the cell. This is relatively straightforward to answer, because the biochemical reactions in energy metabolism of the muscle have been investigated intensively. Phosphate is transferred from

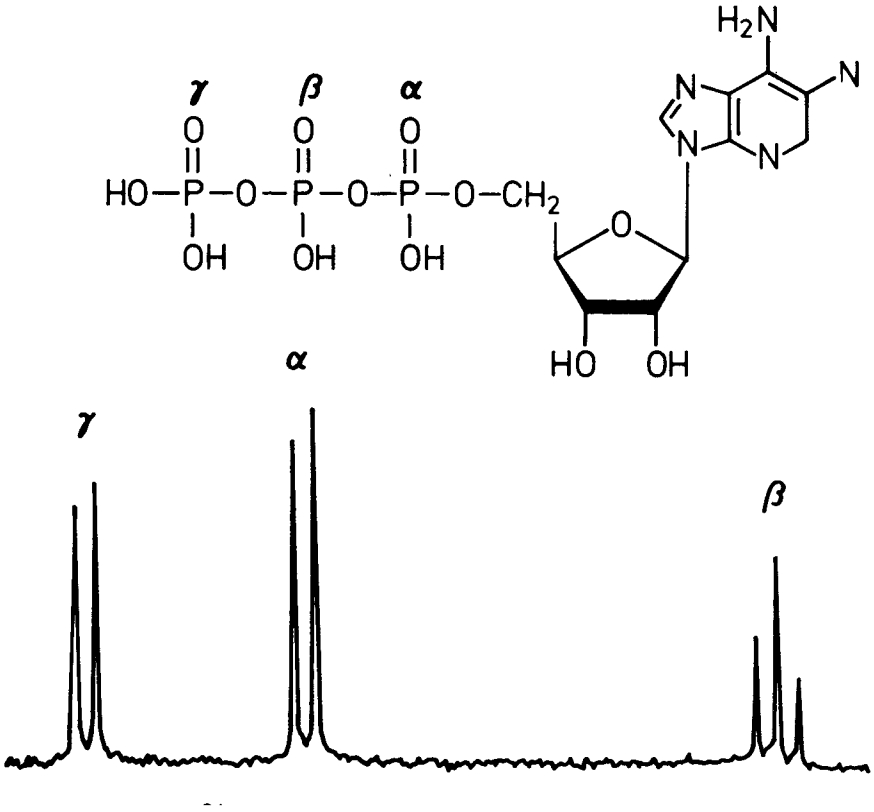

^{31}P-NMR spectrum of adenosine triphosphate at 49.58 MHz with phosphorous acid as a reference. The peak assignment is according to the annotation of the structure above. The nuclei are coupled and Dublets and Triplets are observed.

Figure 6.27 ^{31}P-NMR spectrum of adenosine triphosphate.

creatin phosphate (PCr) to adenosine diphosphate (ADP) to form adenosine triphosphate (ATP) and creatin (Cr). The ^{31}P-NMR spectrum of ATP is shown in Figure 6.27. The nuclear spin of ^{16}O is zero and therefore the ^{31}P-NMR lines are split only by 2 *J* coupling between the phosphorous nuclei. P_α and P_γ are split into a doublet while P_β is split into a triplet, due to the coupling with two neighbor nuclei. The resonance lines of ATP are clearly observed by their chemical shifts and by their relative signal intensities also in the spectrum of a human forearm Figure 6.27. This spectrum contains two additional resonance lines, that of

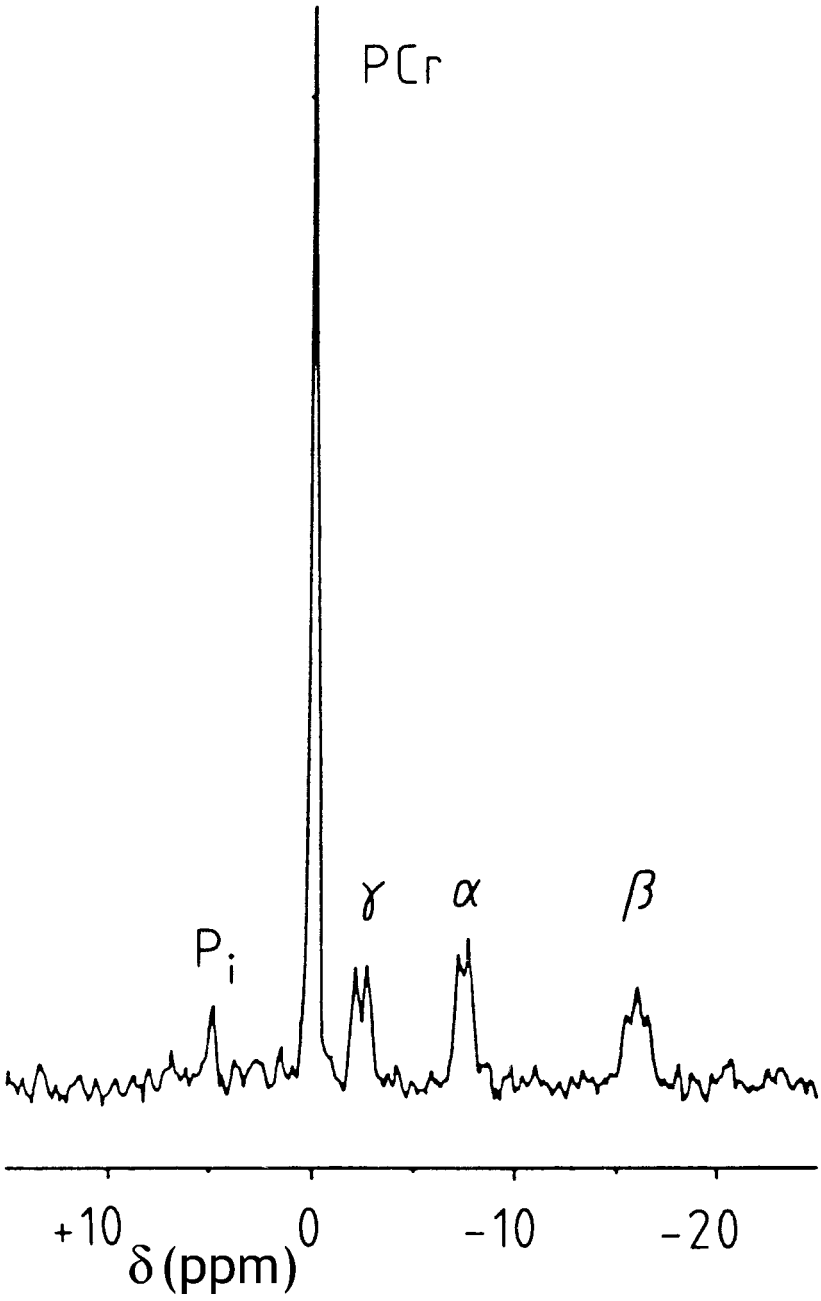

Figure 6.28 ^{31}P-NMR spectrum of a human forearm.

creatine phosphate (PCr) and that of free phosphate (Pi). Signals of ADP, that is also present, are located below the signals α and γ of ATP. The signals of other phosphor organic compounds disappear in the background noise of the spectrum. The signal from the human forearm is dependent on the condition. It will be different if the arm has rested or was used in hard work

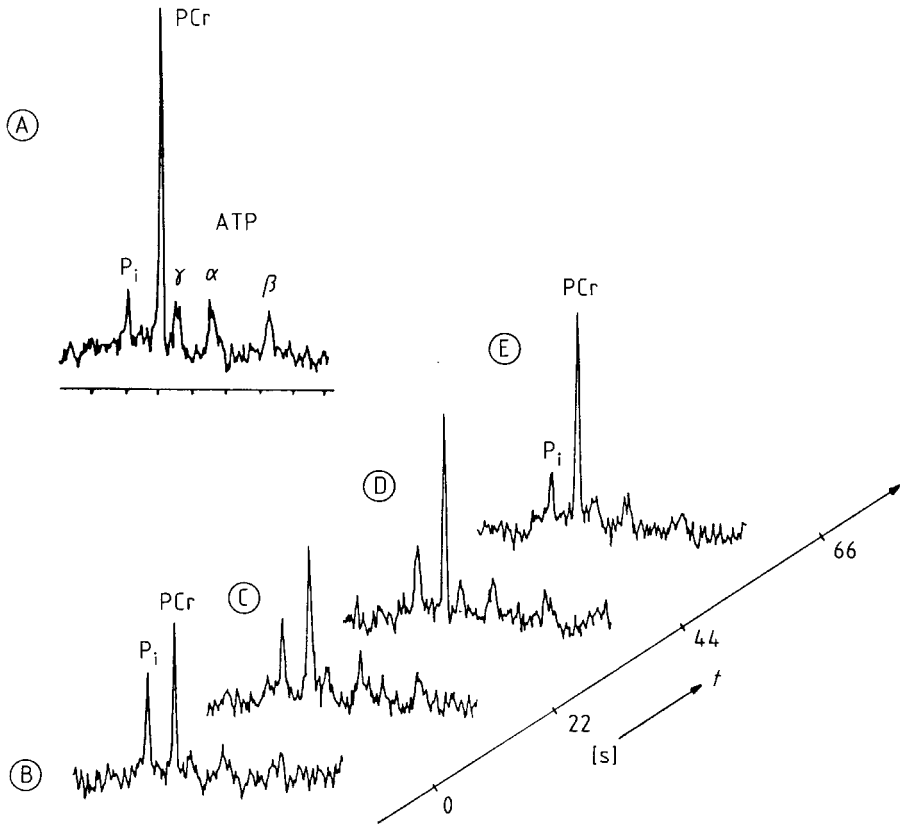

Sequence of ^{31}P-NMR spectra of a human forearm after 10 min of hard excercise. 40 MHz spectra were recorded with a surface coil of a diameter of 4 cm. 10 scans were accumulated per spectrum. The spin system was allowed to relax for 2 s. The total time required to record one spectrum was 22 s. The control spectrum (A) was recorded before the excercise. The patient then had to squeeze a ball outside the magnet until he was unable to continue. The spectra B to E were recorded after completion of the excercise.

Figure 6.29 Spectra of the human forearm as a function of physical stress.

or exercise. Figure 6.29 displays the spectrum of the forearm at rest (A) and at different times after exposure to physical stress. Immediately after performing work, the signal of PCr is reduced, while the spectrum of the inorganic phosphate is strongly increased. After 66 s the original concentrations of all compounds are restored and the spectrum corresponds to the spectrum in the resting condition. The ratio of the organic phosphorous compounds has changed relative to the relaxed state after the forearm was exposed to a physical stress

condition. More dramatic effects are found, if the muscle had a reduced supply of oxygen over a longer time (ischemia). This is possible, if the bloodstream is reduced by a constriction of the blood vessels. The most prominent example is the myocardial infarction (ger.: Herzinfarkt).

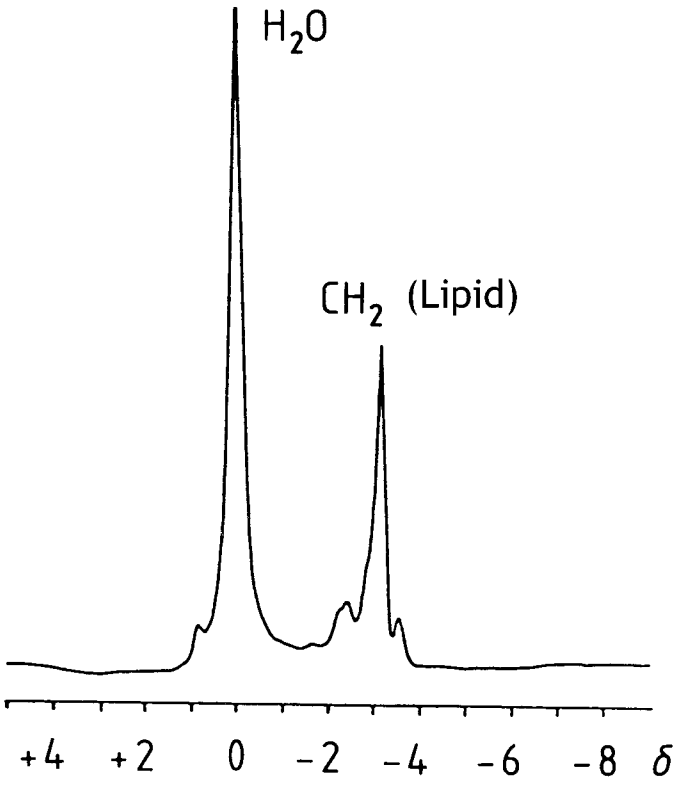

100 MHz ^{1}H-NMR spectrum of the human forearm. The major signals are that of water and that of methylene protons of lipids. The δ-scale shown here is based on water as the standard. 2 scans were averaged. Acquisition time: 5 s.

Figure 6.30 ^{1}H-NMR spectrum of the human forearm.

6.9.1.1 ^{13}C and ^{1}H NMR spectroscopy in vivo.

Problems that have to be overcome for in vivo applications of ^{13}C and ^{1}H NMR spectroscopy are

- a large variety of mixed organic compounds are present, often of highly complex molecules.
- organic substances in the body are often present at very low concentrations.

- the solvent water

- small chemical shifts in ^{1}H-NMR spectroscopy.
- broad lines as a result of field inhomogeneities.

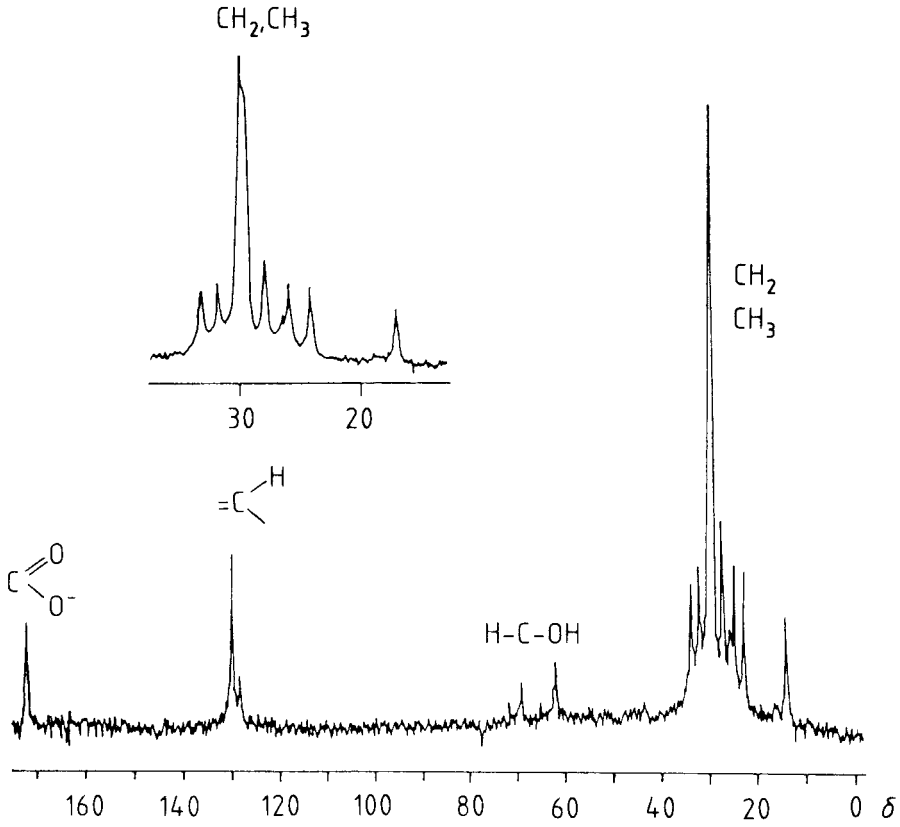

25 MHz broad-band decoupled ^{13}C-NMR-spectrum of the human forearm. 500 scans were averaged (acquisition time: 10 min). Signals must be assigned to the carbon atoms of lipids (glycerol. and fatty acids).

Figure 6.31 ^{13}C-NMR spectrum of the human forearm

Figure 6.30 shows the ^{1}H-NMR spectrum of the human forearm. Two signals dominate the spectrum. The first is a strong absorption line of water, that is also used as a reference in the chemical shifts of other molecules in *in vivo* ^{1}H-NMR spectroscopy. The second resonance line is that of the methylene group that is present in the lipids of the body. Most other signals are of negligible intensity.
More information can be obtained from ^{13}C-NMR spectroscopy. Figure 6.31 shows the ^{13}C-NMR spectrum of a human forearm. Since the chemical shifts of ^{13}C are relatively large, the signals of the lipids in the forearm can be distinguished. The carboxy-groups have the largest chemical shift (δ=172). Chemical shifts of δ=130 for the carbons that participate in a double bond, δ=60-75 for the carbon atoms of the glycerol backbone, and δ=10-35 for the carbons of the aliphatic fatty acids signals are observed. For the spectrum shown in Figure 6.31 it was necessary to accumulate 500 scans and the total acquisition time for the spectrum was 10 min. In modern investigations, organic compounds enriched in ^{13}C are used.

6.9.1.2 Magnetic resonance tomography.

Because of their high sensitivity, the in vivo NMR spectroscopy of the protons was developed further. Since living systems are always containing water, the distribution of water in the organism was investigated first. For small volume elements that contain lots of water, stronger signal intensities were expected than for those small volume elements that contain relatively little water. The problem therefore was, to develop a method to measure the distribution of water in the body by ^{1}H-NMR spectroscopy. Three technical problems had to be addressed:

- The size of the magnet. For example, if the water distribution in a human head must be determined then the magnet has to have an opening large enough for the head. In conventional high resolution NMR spectrometers, this opening is only a few cm wide. This problem is solved nowadays and electromagnets with a magnetic field strength of up 0.3 T are used. Sometimes even cryomagnets with a field strength up to 3 T are part of in vivo NMR tomographs.
- The second problem is also a technical difficulty, that must be overcome. The resonance condition must be fulfilled to obtain an NMR signal and this is difficult for a heterogeneous large object like a human head. In NMR tomography, only small volume elements are analyzed in which a local field B_0 is generated. In theses volume elements (*voxels*) the resonance condition is met in the inside but not in the outside or in their surface regions. For a fine resolution these voxels need to be small. The disadvantage of smaller voxels is the reduced signal intensity due to a smaller number of ^{1}H nuclei. The data acquisition time is therefore the longer the smaller the volume element. With mice and other small animals the highest spatial

resolution corresponds to a volume element of 10x10x100 µm. The imaging with such a high resolution is termed NMR microscopy, although the resolution of optical spectroscopy is not yet matched by NMR microscopes. The selection of the volume element is achieved by magnetic fields that have a variable gradient of the magnetic field strength. With these magnetic field gradients, slices of different magnetic field strengths are formed through the object. These slices are subsequently divided into small volumes. Usually, these slices are about 7 mm thick and single volume elements are rods of 1 mm diameter and a length of about 7 mm. To image the complete head, at least 8 such slices are necessary. The result of NMR-absorption of each volume element is registered, stored, and converted into a signal by Fourier transform spectroscopy.

- The third problem is that of imaging (reconstruction of the image from the individual measurements on each voxel). This problem could be solved in analogy to the experiences obtained from x-ray tomography. Today it takes only a few seconds to measure the water distribution in a particular object.

From the medical point of view, the distribution of water is not all that exciting. More interesting became the magnetic resonance tomography by the fact that the relaxation times T_1 and T_2 depend characteristically on the environment of the water, i.e. on the tissue to which the water is bound. The images that are required therefore should reflect not only the density distribution of water, but also the changes in the relaxation times T_1 and T_2.

We have previously discussed how one can obtain the relaxation times T_1 and T_2 by pulse sequences 90°-τ-180° (T_2) and 180°-τ-90° (T_1). The spin-system relaxes after a 180° pulse with T1 and the intensity of the signal will be zero after a time $\tau=T_1$ ln (2) s. Nuclei with different T_1 time have a different time τ at which the signal intensity becomes zero. This is also true for protons in water, if the T1 times are not the same because of different environment of the water molecules in different tissues. At any given time t, the images obtained will differ in contrast or color.

A similar dependence on location of the water is also observed for the spin-spin relaxation time, T_2. Two illustrate the dependence of T_2 on the water density, a spin-echo experiment is performed. The regions of different contrast in the image indicate a distribution of different spin-spin relaxation times. The quality of the images is comparable to that of an x-ray tomogram, and maybe even of better quality in some cases. The NMR experiment has one big advantage: It does not expose the body to damaging x-ray radiation. In this way, the experiments may be repeated without danger. Risks for the human health imposed by magnetic fields or by switching them on and off are currently not known.

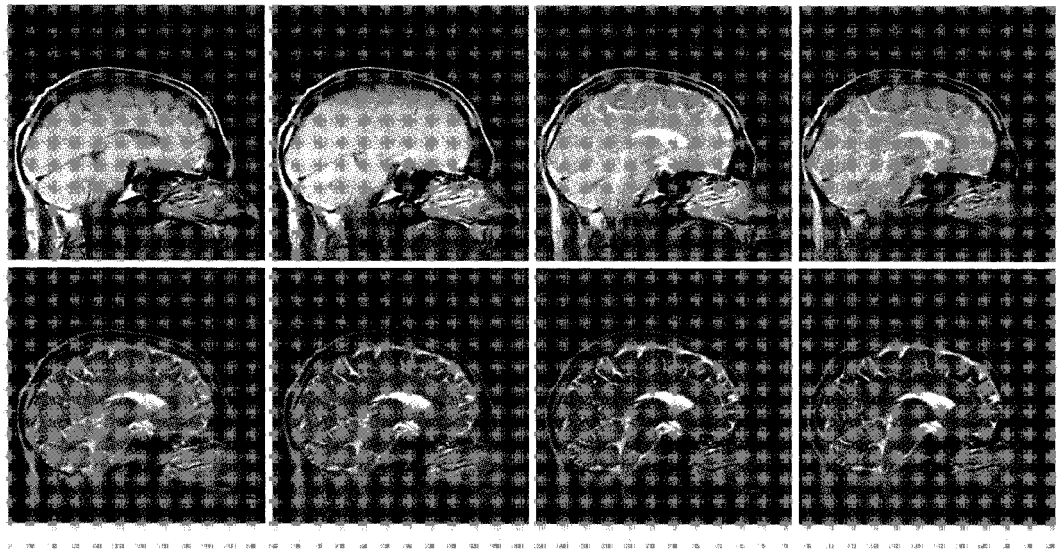

Medio-Sagittal cut through the skull. In this experiment, a multiple echo sequence was used in which 8 echos were recorded. Each image of this series corresponds to one of the 8 echos. In each image, the same slice of 7 mm thickness is shown, which was devided into 256 x 256 matrix elements . For each matrix element, two spectra (FIDs) were accumulated. The total acquisition time for the eight images was about 11 min. (The images were recorded on a NMR tomograph of the Company Bruker, Rheinstetten, Karlsruhe, with a cryo-magnet at a field strength of 1.5 T.)

Figure 6.32 NMR Tomography of a human skull. Each image corresponds to a spin-echo.

Figure 6.32 shows 8 images of a medio-sagittal slice through a human skull. A slice of 7 mm thickness was recorded. The pulse sequence that was used in this experiment is shown in

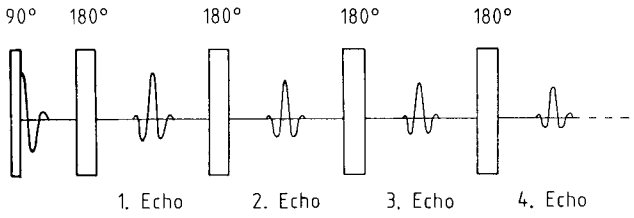

Multiple echo sequence after Carr-Purcell-Meiboom-Gill. The first 90° pulse prepares the spin system, the following 180 °pulses generate the echos. For skull imaging, 8 such echos were recorded.

Figure 6.33 Multi echo sequence after Carr-Purcell-Meiboom-Gill. The first 90° pulse prepares the spin-system, the following 180° pulses generate the echoes.

Figure 6.33 . Each of the 8 images shown in Figure 6.32 corresponds to one of eight echoes. The first image very closely corresponds to the effective water distribution in the skull (light contrast corresponds to water rich regions, dark contrast to to relatively little water) The series of images shows that the contrast changes from echo to echo and the contours become

better visible. The changes in contrast are a direct consequence of the different spin-spin relaxation times T2 in the different types of tissues of the brain. It is also visible that the overall brightness of the image is reduced from the first to the last image due to relaxation. Between excitation and the 8th echo a time of 0.3 s has passed. The complete time for the recording of the 8 echoes was 11 min.

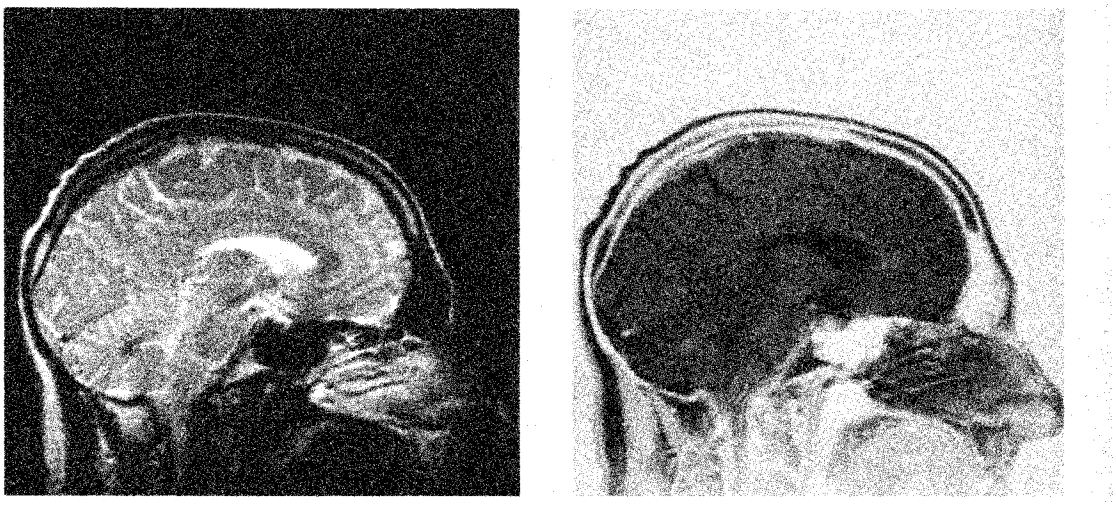

Figure 6.34 A sum of the eight images shown in Figure 6.32 . B Negative of A, showing the bones in white color.

In Figure 6.34 A, the sum of the 8 echoes shown in Figure 6.32 is shown. This representation will give images that are very rich in contrast. In Figure 6.34 B the negative is shown, that is also computer generated. In the negative image the bones have white color. In Figure 6.35 , one matrix element (voxel) is marked and the relaxation time T_2 can be obtained from the intensities in each of the eight echoes of Figure 6.32 . It is usually also calculated by the computer (T_2=101 ms in this case).

In medical applications it is of importance that the relaxation times T_1 and T_2 are very different between healthy and unhealthy tissue.